superposition four semi infinite solenoids produces the same field function as the finite solenoid (Figure 73b). If the field component (radial or axial) of the solenoids is H_1, H_2, H_3, H_4, from the same sensed current density rotation, then the desired thick solenoid field is

$$H = H_1 - H_2 + H_3 - H_4 \tag{72}$$

Dividing by the current density J and the inner radius s, equation 72 is nondimensionalized:

$$\frac{H}{Js} = \frac{H_1}{Js} - \frac{H_2}{Js} + \frac{H_3}{Js} - \frac{H_4}{Js}$$

With semiinfinite solenoid radii b_1, b_2, b_3, b_4, where $b_3 = b_4 = s$, and $b_1 = b_2 = \alpha s$, and if quantities such as $H_1/Jb_1 = h_1$ etc,

$$\frac{H}{Js} = \alpha h_1 - \alpha h_2 + h_3 - h_4 \tag{73}$$

Each solenoid value is nondimensionalized by its outer radius as a unit of length, working from the centre line and end face, as shown in Figure 73b. Although Brown and Flax give both graphical and tabular solutions for h, in radial and axial directions, their integrals can also be evaluated on a programmable calculator.

3. Rectangular Coils

3.1 Line Filament Solutions

As with circular coils, a line filament solution represents an easy first approximation to a finite section coil, especially when the required field point is some distance away. For close field points, a filament solution can still be used if it is based on a geometric mean distance (GMD) approximation of the finite coil build (Figure 74). The field expressions derive from the Biot-Savart relationship applied to the current element dl, which carries a current I and produces an elemental field dB at the origin of an orthogonal coordinate set. s is the vector from the current element to the origin

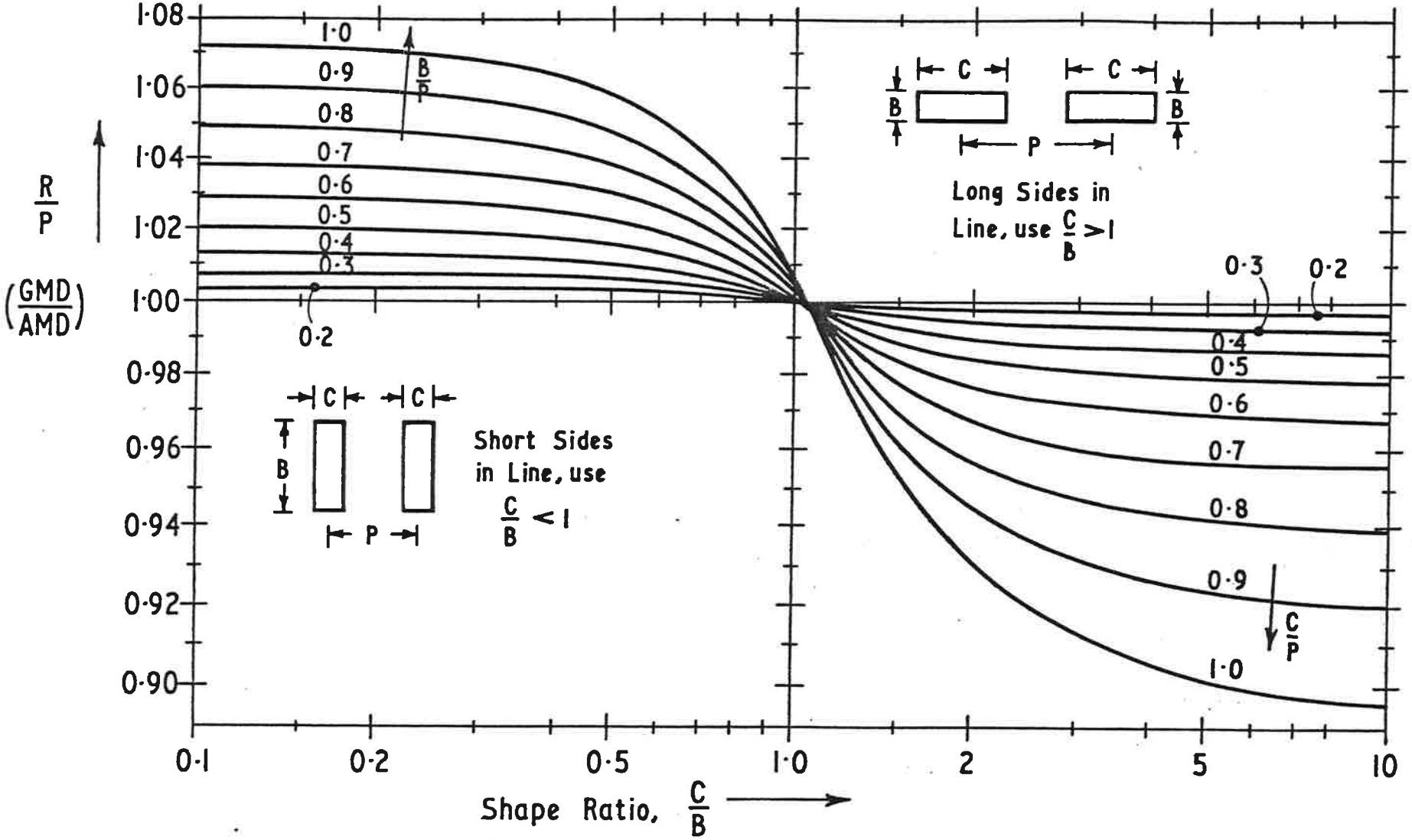

Figure 74. Geometric/Arithmetic Mean Distance for Equal Parallel Rectangles.

(Figure 75). The field is given by

$$\underline{dB} = \frac{\mu_0 I}{4\pi} \frac{\underline{dl} \times \underline{s}}{|\underline{s}|^3}$$

Evaluation produces the result

$$\underline{dB} = \frac{\mu_0 I}{4\pi} \frac{(y\hat{i} - x\hat{j})\,dz}{(x^2+y^2+z^2)^{3/2}} \qquad (74)$$

If the coordinates are chosen so that the z axis is parallel to a current filament of finite length, starting at coordinate z_1, and finishing at z_2, the x and y values of field at the origin can be found by using 74. Montgomery has incorrectly stated the expressions for this case[262], they should be written as

$$B_x = \frac{\mu_0 I y}{4\pi(x^2+y^2)} \left[\frac{z_2}{(x^2+y^2+z^2)^{1/2}} - \frac{z_1}{(x^2+y^2+z^2)^{1/2}} \right]$$

$$B_y = \frac{-\mu_0 I x}{4\pi(x^2+y^2)} \left[\frac{z_2}{(x^2+y^2+z^2)^{1/2}} - \frac{z_1}{(x^2+y^2+z^2)^{1/2}} \right] \qquad (75)$$

The assumption is that positive current flows in the positive z direction. By using 75, the on and off axis fields of rectangular coils can be easily calculated. Volume superposition can be used (Figure 76) with integration of 74 to find the finite section field, although this is treated in more detail later. For the on axis case, if the coil has a base width of 2e and breadth of $2\gamma e$, the on axis field at a height $z = \delta e$ below the coil is given by

$$B_z = \frac{\mu_0 I}{\pi e} \frac{\gamma}{(\gamma^2+\delta^2)(1+\delta^2)} \cdot \frac{1+\gamma^2+2\delta^2}{(1+\gamma^2+\delta^2)^{1/2}} \qquad (76)$$

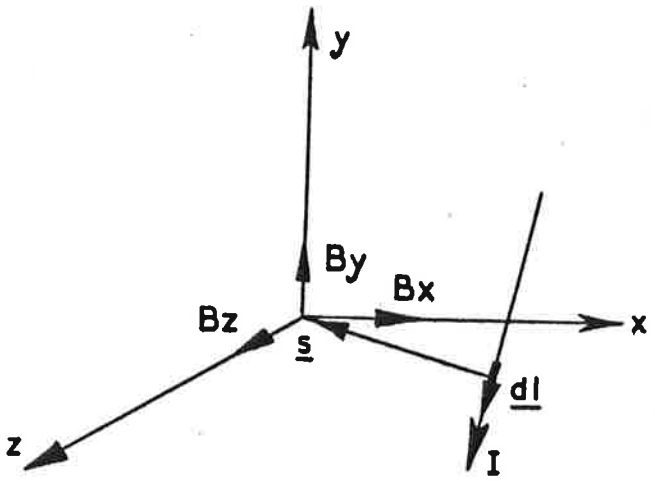

Figure 75. Current element dl

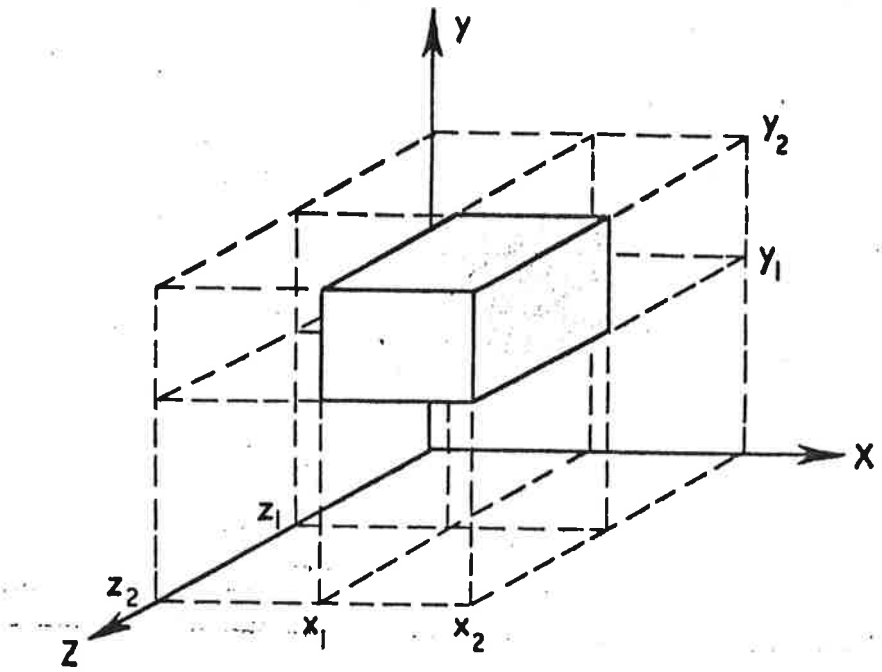

Figure 76. Volume superposition.

The central field (z = 0) is simply

$$B_0 = \frac{\mu_0 I}{\pi e} \left(1 + \frac{1}{\gamma^2}\right)^{1/2} \qquad (77)$$

Figure 77 shows the axial field variation for various heights and width to breadth ratios. The circle with the same radius as the coil half width is given for comparison.

The off axis field profile is indicated for a square coil by Figure 78 which is a plot of the vertical field for a point equidistant from two of the coil sides, at various heights. The shape of the profile indicates the high harmonic content of the flux variation when a magnet array is made up of alternating coils at levitation heights much less than the coil half width. The rapid fall off of field as the reference point moves under the transverse coil side is also readily apparent.

3.2 Finite Sections

The rectangular coil with finite section is more difficult to successfully evaluate. For general field points away from the actual wound section, and indeed for the central field itself, the coil limbs can often be approximated by the finite length rectangular bar equivalent. Figure 79 shows, for example, how a square coil can be split into bar equivalents to include the corner sections. A corner overlay of adjacent bars would accommodate the rapid change on direction of current at the corner more successfully. For the case when very long coil sides are present, the infinitely long rectangular bar can be used with superposition as in Figure 79 to evaluate field values. Figure 80 shows an infinitely long rectangular bar, with one edge running along the z axis. The field components B_x and B_y at the origin (B_z = 0) are given by the expressions shown. Essentially equation 74 can be double integrated over the x and y limits from 0 to +x and +y. Normalizing by the x value (i.e. to give a bar of unit width and height $\gamma = \frac{y}{x}$)

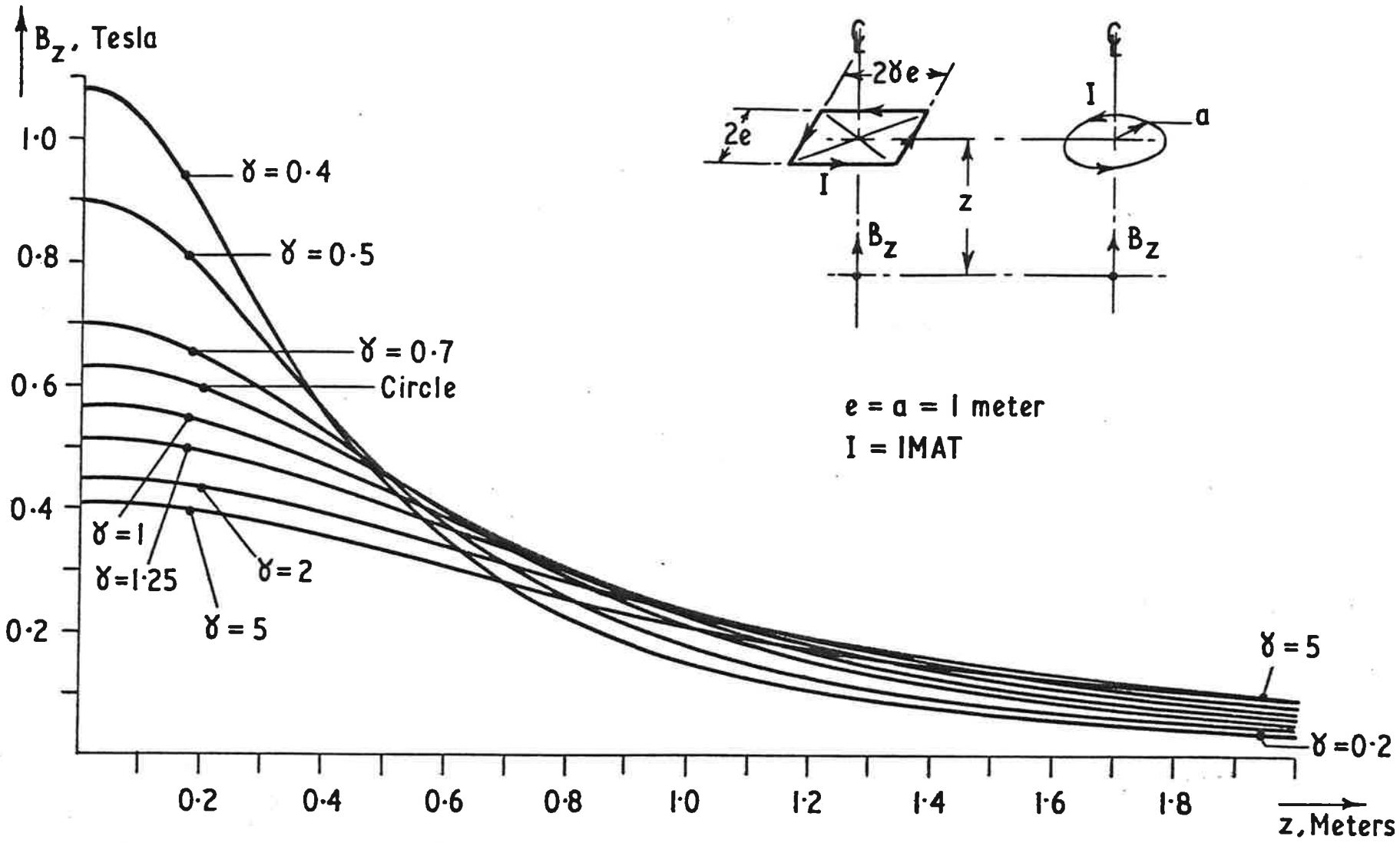

Figure 77. Axial Field Variation at Height z for Rectangular and Circular Coils.

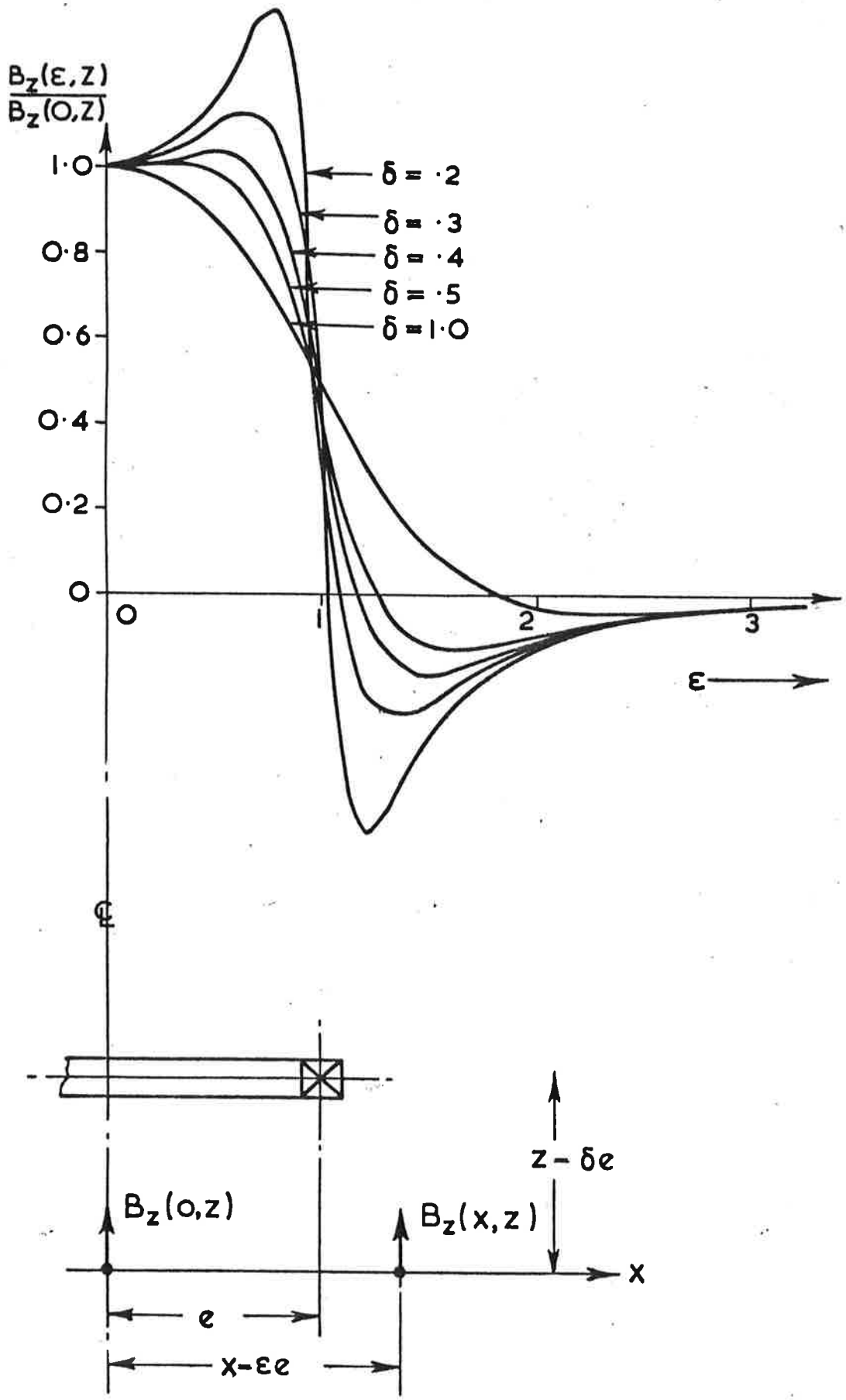

Figure 78. Normalized lateral field variation for a single turn square coil.

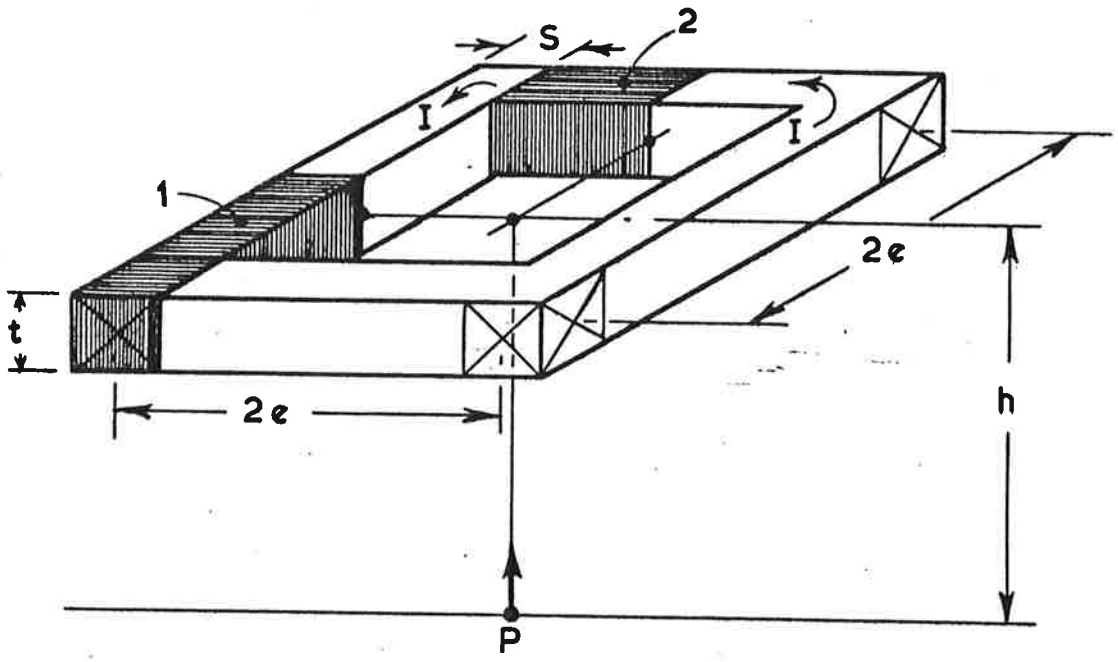

a) Subdivision of square coil for on-axis field.

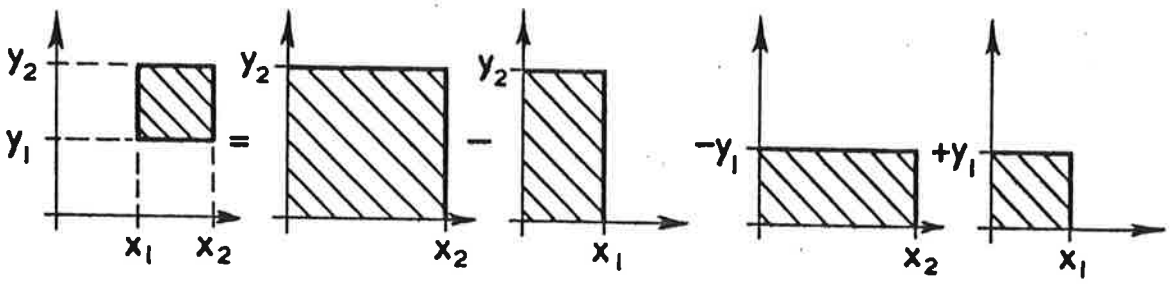

b) Superposition principle for off-corner field points.

Figure 79. Field at a point for finite section coils.

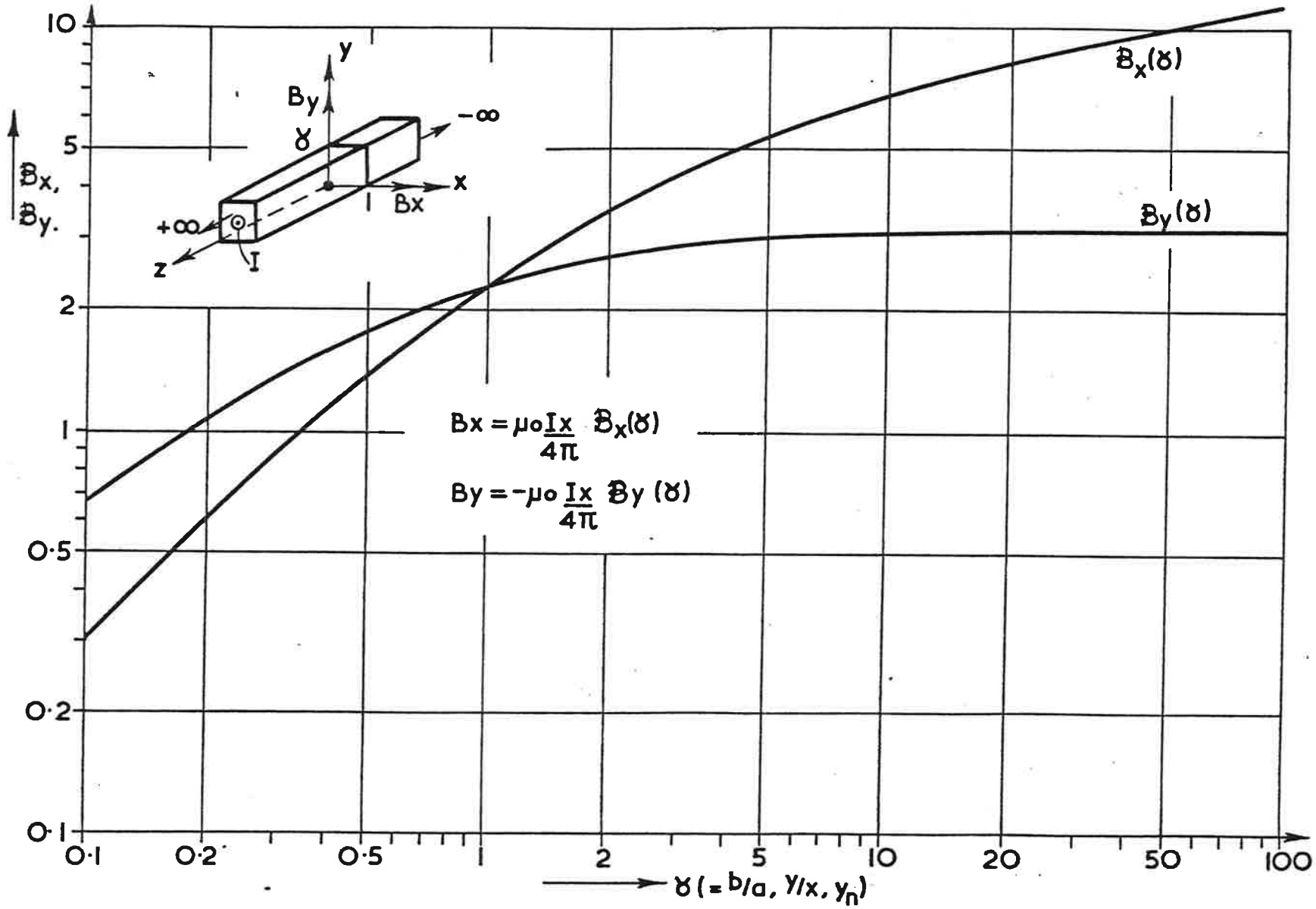

Figure 80. Field functions for unit width infinitely long rectangular bar.

produces field values

$$B_x = \frac{\mu_0 I x}{4\pi}\left[\ln(\gamma^2+1) + 2\gamma\tan^{-1}\left(\frac{1}{\gamma}\right)\right]$$

$$B_y = -\frac{\mu_0 I x}{4\pi}\left[\gamma\ln\left(1+\frac{1}{\gamma^2}\right) + 2\tan^{-1}\gamma\right] \qquad (78)$$

The field functions are the values within square brackets and are plotted in Figure 80 for various shape ratios γ. Superposition as demonstrated by Figure 79 allows the field components distant from a infinitely long rectangular bar to be determined.

Similar field functions can be obtained for finite length rectangular bars. Here the bar stretches from the origin to a finite value of z, and similarly has one edge aligned to the z axis, in the positive quadrant of x and y. Triple integration of 74 and normalizing the coordinates by x to give unit width and bar height $y_n = \frac{y}{x}$ and bar length $z_n = \frac{z}{x}$, with I replaced by $j\lambda\, dydx$ ($j\lambda$ is the overall current density), produces

$$B_x = \frac{\mu_0 j\lambda x}{4\pi}\mathfrak{B}_x^*$$

$$B_y = -\frac{\mu_0 j\lambda x}{4\pi}\mathfrak{B}_y^* \qquad (79)$$

where

$$\mathfrak{B}_x^* = z_n \ln\left[\frac{[1+(1+z_n^2)^{1/2}][1+\frac{y_n^2}{z_n^2}]^{1/2}}{1+(1+y_n^2+z_n^2)^{1/2}}\right] + \ln\left[\frac{[z_n+(1+z_n^2)^{1/2}][1+y_n^2]^{1/2}}{z_n+(1+y_n^2+z_n^2)^{1/2}}\right] + y_n\tan^{-1}\left[\frac{z_n}{y_n(1+y_n^2+z_n^2)^{1/2}}\right]$$

$$\mathfrak{B}_y^* = z_n \ln\left[\frac{[y_n+(y_n^2+z_n^2)^{1/2}][1+\frac{1}{z_n^2}]^{1/2}}{y_n+(1+y_n^2+z_n^2)^{1/2}}\right] + y_n \ln\left[\frac{[z_n+(y_n^2+z_n^2)^{1/2}][1+\frac{1}{y_n^2}]^{1/2}}{z_n+(1+y_n^2+z_n^2)^{1/2}}\right] + \tan^{-1}\left[\frac{y_n z_n}{(1+y_n^2+z_n^2)^{1/2}}\right] \qquad (80)$$

Figure 81 and 82 plot the field functions given by equations 80 for the unit width normalized height and length bars, and have also been transferred to a programmable calculator.

4. Racetrack Coils

Field solutions for finite section racetrack coils usually require a complex program which will present finite element approximation to the coil dimensions using a standard suite of building bricks or generated volumes. A filamentary approximation is however possible, using a combination of formulae for finite length straight wires and a field solution for a filamentary quadrant or half circle. Figure 83 shows how the coil sides are broken into four groups to enable the field components to be evaluated. If the coil has straight elements on all four sides, then a quadrant field expression (rather than semi-circle) must be used for each of the corner radii.

Figure 84 shows a coordinate set for evaluating the field at a point P produced by a quadrant of a circular current filament. P is chosen to lie on the x axis, and the Biot Savart expression is used with the appropriate vectors to give the three field components. If the limits on α are chosen to be $\pm \frac{\pi}{4}$ instead of 0 and $\frac{\pi}{2}$, then B_y is zero, and with the coil elevation z and radius r normalized by the offset of P from the coil centreline, h so that

$$z = hZ$$

$$r = hR$$

then

$$B_x = -\frac{\mu_0 I}{2\pi h}\int_0^{\pi/4} \frac{RZ\cos\alpha \, d\alpha}{(1+R^2+Z^2-2R\cos\alpha)^{3/2}}$$

$$B_z = +\frac{\mu_0 I}{2\pi h}\int_0^{\pi/4} \frac{(R^2 - R\cos\alpha)\, d\alpha}{(1+R^2+Z^2-2R\cos\alpha)^{3/2}} \qquad (81)$$

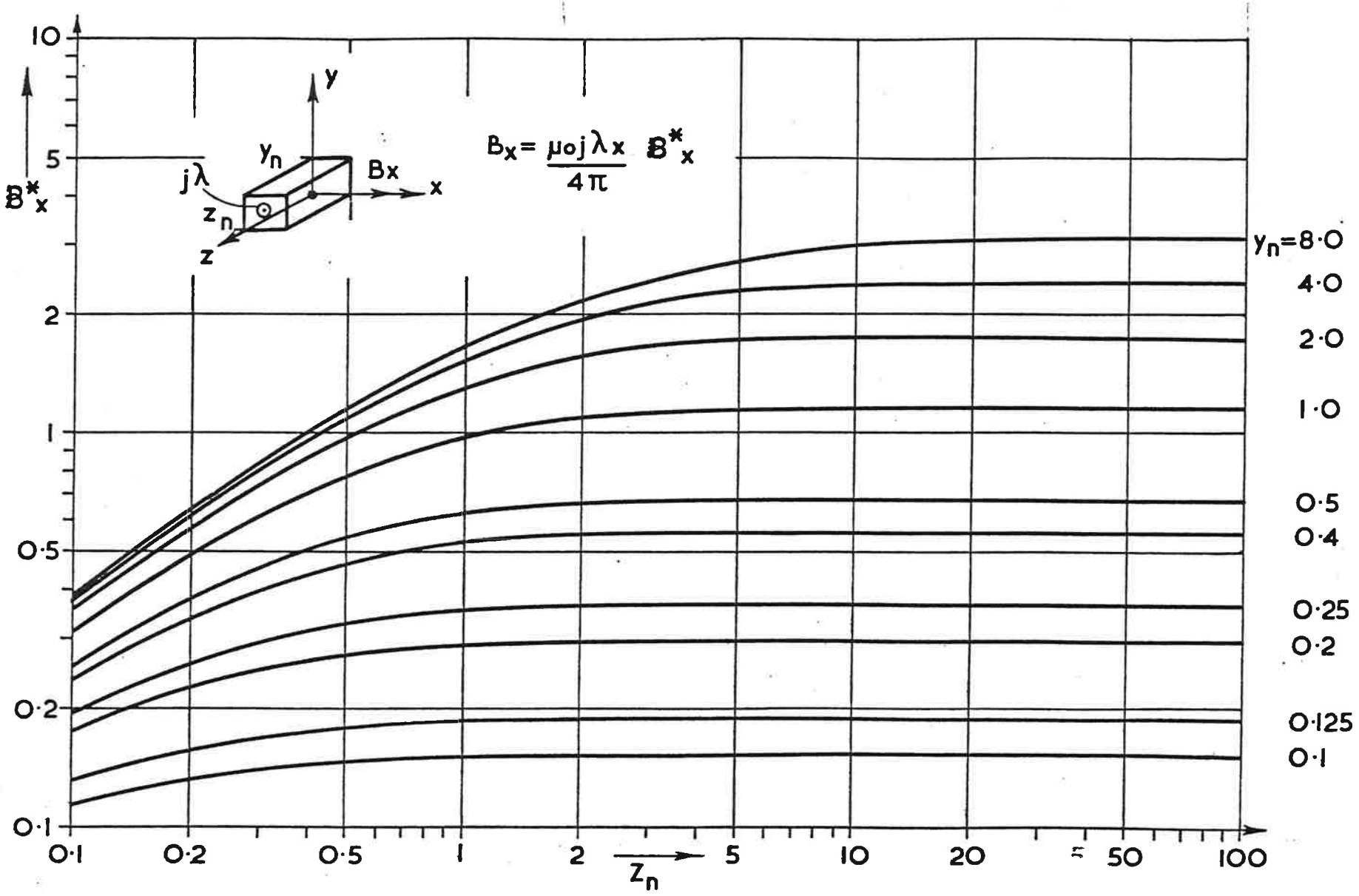

Figure 81. Field functions for unit width finite length rectangular bar.

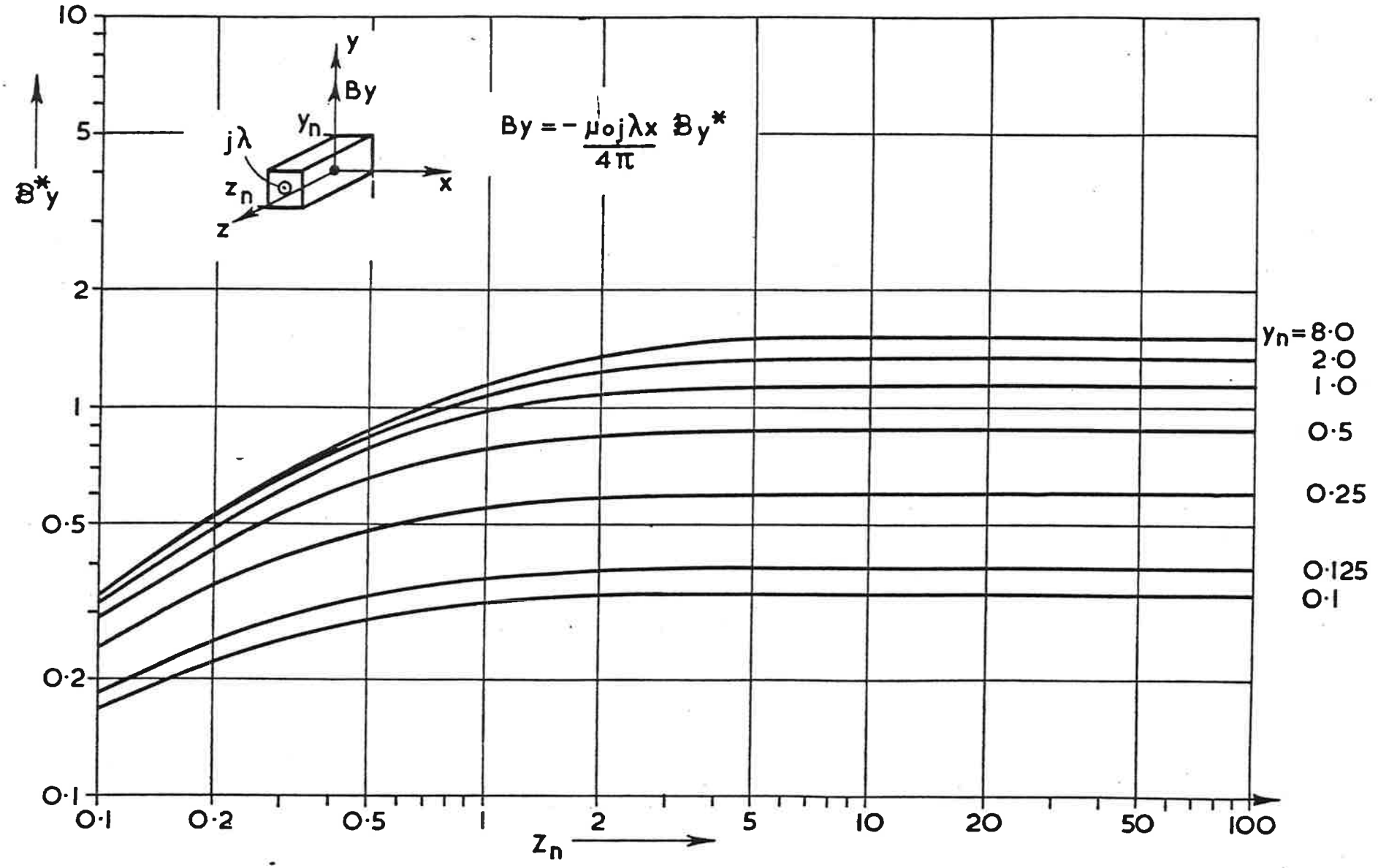

Figure 82. Field functions for unit width finite length rectangular bar.

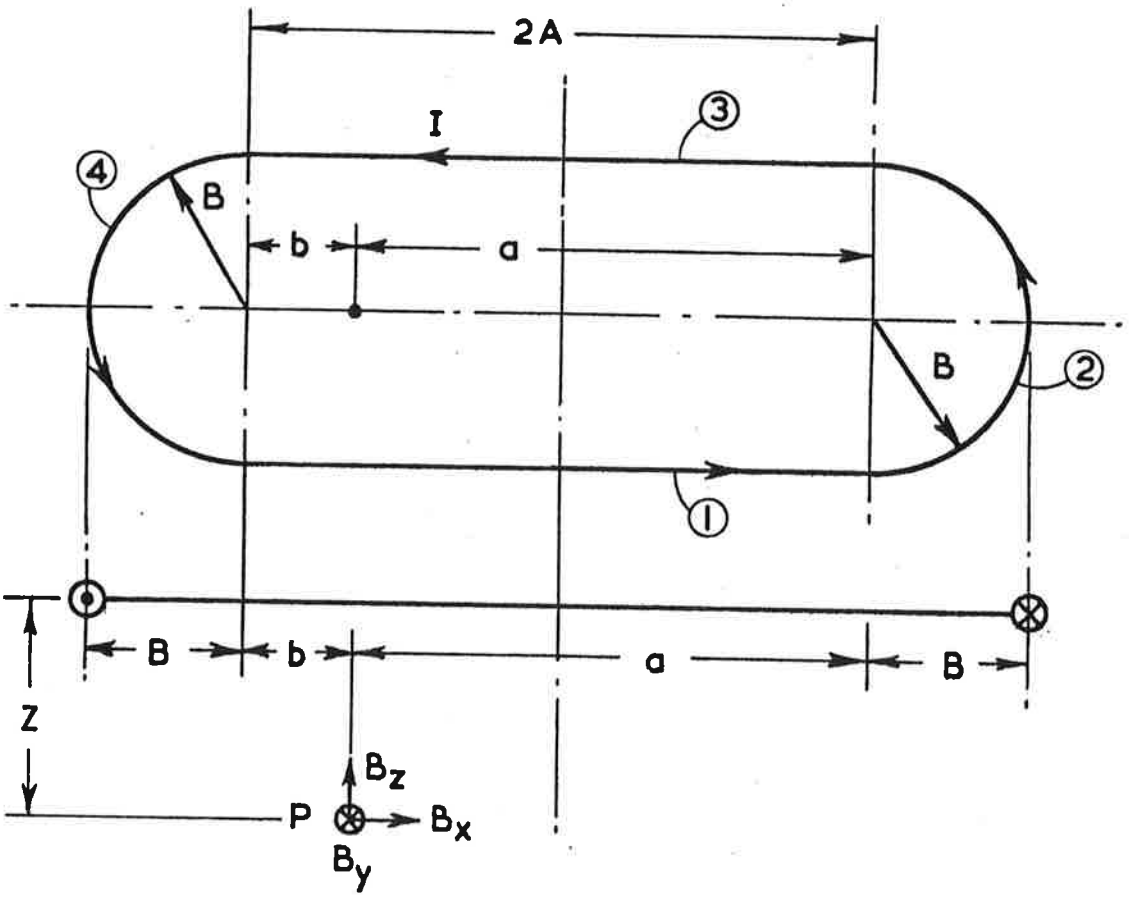

Figure 83. Race-track coil field components, off axis.

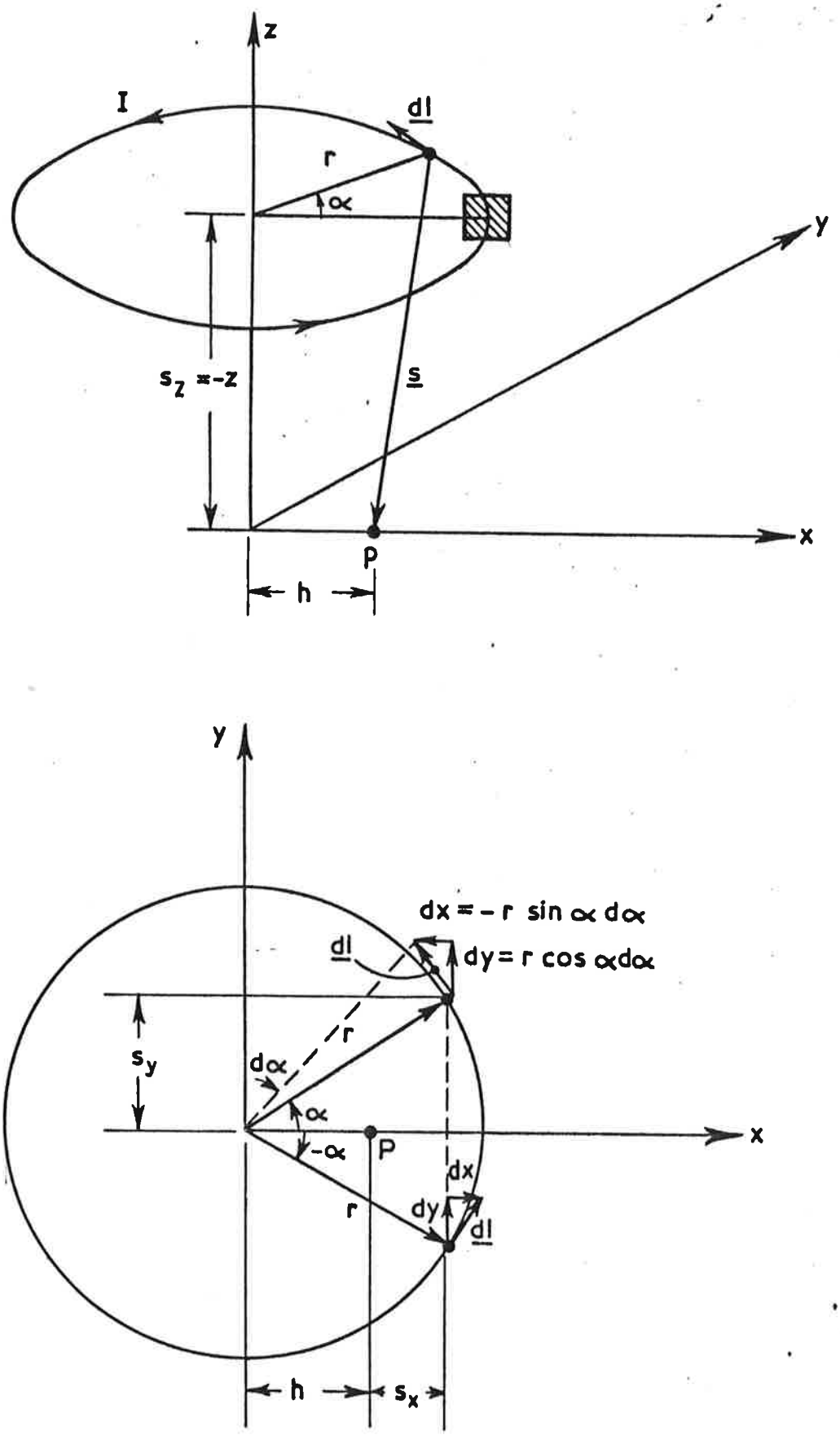

Figure 84. Off-axis field for quadrant of a circular current filament.

Equation 81 can be evaluated after some manipulation as expressions involving incomplete elliptic integrals of the first and second kind, but requiring only values of Z and R to define the modulus and argument. This technique was used to evaluate the central fields of finite corner radius rectangular coils discussed in 3.4.

APPENDIX III

DERIVATION OF TRACK INDUCTANCE

APPENDIX III DERIVATION OF TRACK INDUCTANCE

1. Introduction

This appendix gives details of the derivation of initial and asymptotic self and mutual inductances as discussed in section 3.2.2. Calculation is eased by the use of superposition, which is valid since the winding is air cored and magnetically linear. The essence in calculating both self and mutual inductance of either single or double layer meander windings is the concept of an elemental inductance of a track segment of one phase, which is one pole pitch long. Calculation of the per unit track length self inductance of this half wavelength element, and then the subsequent addition of adjacent elements, yields a series, which for a double layer winding converges to a finite value. The additional terms which are far from the initial segment can be represented as line filaments, and have characteristics determined by the track width to pole pitch ratio. The whole expression splits into two terms which relate to the finite size of the winding (i.e. its cross sectional area or aspect ratio, as well as the relevant limb length) and the track width to pole pitch ratio linked with the number of adjacent segment pairs involved (i.e. linked to the track section length). The first term is defined as the initial inductance, since its evaluation centres on the initial elemental segment with no additional side segment contributions. The second term, the asymptotic inductance, is so called since evaluation of the running total of terms involving width to pole pitch ratio and the number of included adjacent segment pairs tends to an asymptotic limit.

The mechanics of the calculation are the same when applied to finding the mutual inductance between two double layer phases. The expressions involve an additional term which is effectively the fractional physical displacement between phases. However, because of the close coupling of the initial

segments, it is necessary to include up to two adjacent segment pairs to each initial element, per phase, into the initial term.

2. Track Inductance

2.1 Phase Leakage Inductance

It is assumed that the track phase winding self inductance can be represented as a summation of the self inductance of an isolated single phase meander winding, and the mutual inductance of the other two (or remaining) phases, reflected into the reference phase. If L_G represents the phase isolated self inductance, and M_G represents the mutual contribution from another phase, for a section length G, then the total phase leakage inductance is simply

$$L = L_G - M_G \tag{1}$$

since the current magnitudes in the remaining phases combine to a full phase equivalent mutual.

2.2 Elemental Inductance

A track meander phase winding (single or double layer) can be modelled as a concatenation of single pole pitch long elements, as shown in Figure 1(a). For a section length made up of k elements, a particular element e_{j+1} can exist with an elemental complement e_{k-j}, so that both have j elements outboard to themselves. If the self inductance of any element e and the mutual inductance contribution to e from the n elements on both sides of e is defined as the elementary inductance interacting to n, or $L_e(n)$, then the contribution of e_{j+1} and e_{k-j} to the phase total self inductance is

$$L(e_{j+1}) = L_s(e_{j+1}) + M(e_{j+1}).j_L + M(e_{j+1}).(k-j-1)_R$$

and

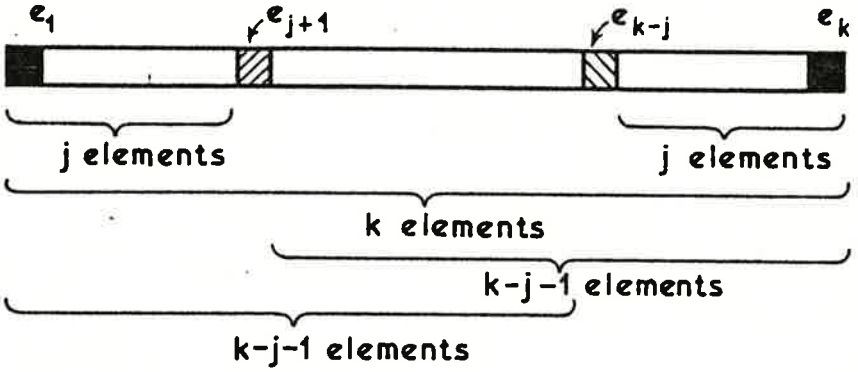

(a) Subdivision of meander winding into pole pitch elements.

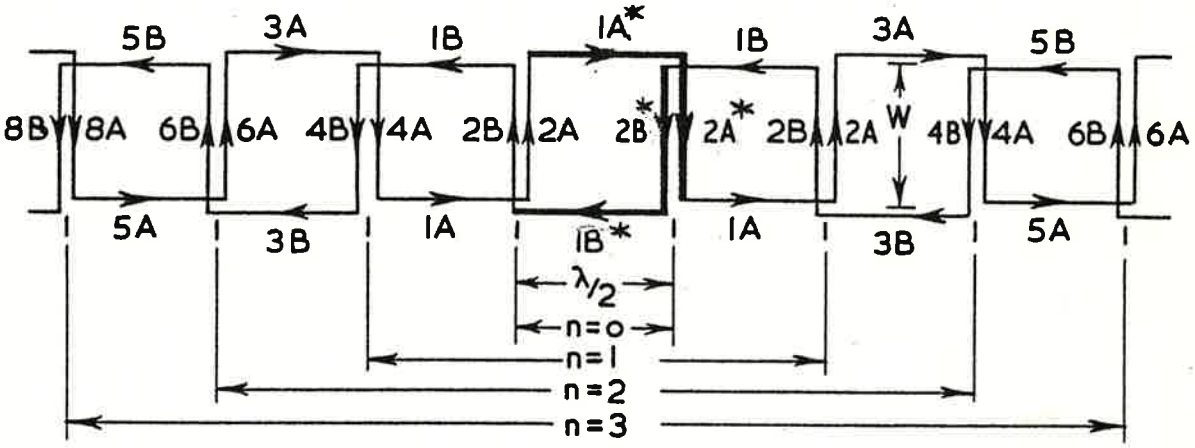

(b) Definition of limbs for self inductance calculation.

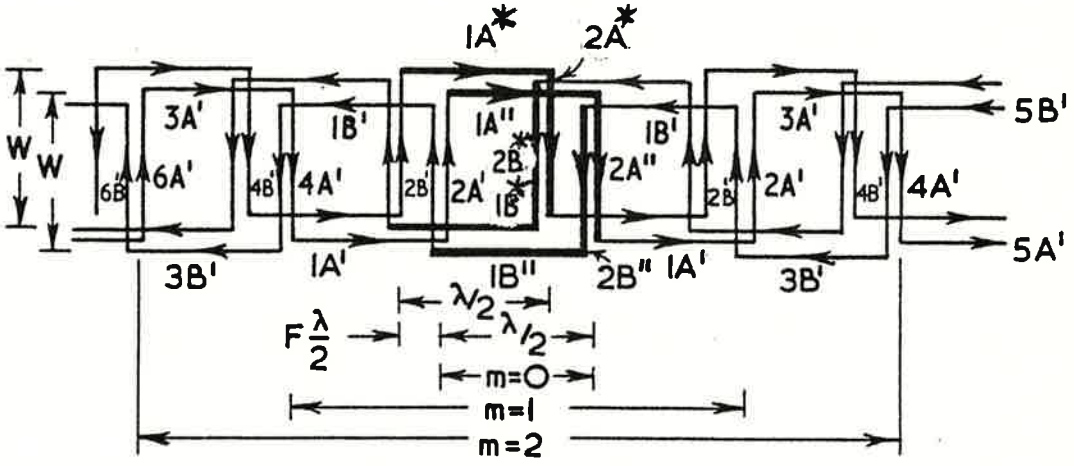

(c) Definition of limbs for mutual inductance calculation.

Figure 1. Armature winding representation.

$$L(e_{k-j}) = L_s(e_{k-j}) + M(e_{k-j}).j_R + M(e_{k-j}).(k-j-1)_L$$

where suffices R and L relate to right and left hand outboard contributions. Adding, and remembering that terms which relate to e_{j+1} and e_{k-j} must be similar,

$$L(e_{j+1}) + L(e_{k-j}) = [L_s(e_{j+1}) + M(e_{j+1}).j_L + M(e_{k-j}).j_R] + [L_s(e_{k-j}) + M(e_{k-j}).(k-j-1)_L + M(e_{j+1}).(k-j-1)_R]$$

so

$$L(e_{j+1}) + L(e_{k-j}) = L_e(j) + L_e(k-j-1)$$

Since the total strip self inductance $L_T(k)$ from k elements is given by

$$L_T(k) = \sum_{i=1}^{k} L(e_i)$$

then

$$L_T(k) = \sum_{n=0}^{k-1} L_e(n) \qquad (2)$$

3. Self Inductance Structure

Equation 2 suggests that the evaluation of the self inductance of an isolated phase winding can be attempted by the successive addition of pole pitches to each side of the initial element. In Figure 1(b) a double layer single phase winding is shown. Limbs 1A* and 2A* represent the 'go' part of the initial element, 1B* and 2B* form the return. The outboard element limbs are then numbered in a progressive sense from the initial element, with the A conductors carrying the go current from left to right, and B conductors carrying return current, a remote half phase connection being assumed.

For the initial element, the reaction with the adjacent segments can be written as

$$L_e = L_L + L_T \qquad \text{(L and T for longitudinal and transverse limb interactions)} \tag{3}$$

By symmetry, the longitudinal interactions to 1A* and 1B* are identical, so

$$L_L = 2L_{L1A} \tag{4}$$

L_{L1A}, the longitudinal interactions to 1A*, is composed of the self inductance of 1A*, L_1, the mutual inductance with 1B*, M_1, as well as the mutual interaction to opposing and colinear longitudinal filaments, from both sides of the initial element.

$$\begin{aligned} L_{L1A} &= L_1 + 2(M_{1B} + M_{3A} + M_{5B} + M_{7A} + \ldots) \text{ colinear terms} \\ &+ M_1 + 2(M_{1A} + M_{3B} + M_{5A} + M_{7B} + \ldots) \text{ opposing terms} \end{aligned} \tag{5}$$

For the transverse terms, only 2A* and 2B* are close coupled. It can be shown that the self inductance, L_2, of two parallel strips 2A* and 2B* with the same current and direction connected in series is equivalent to four times the self inductance of a single strip with double thickness, L_{2A2B}

$$L_2 = 4\, L_{2A2B} \tag{6}$$

Therefore,

$$L_T = L_2 + 8(M_{2A} + M_{4A} + M_{6A} + M_{8A} + \ldots) \tag{7}$$

However note that for n=0, only L_2 is involved, and for n=1, L_2 is added to $8M_{2A}$ and $4M_{4A}$. The next step n=2 adds $4M_{4A}$ and $4M_{6A}$.

The way in which $L_e(n)$ is generated is established by using equations 3-7

$$L_e(n) = 2(L_1 + M_1) + L_2 + 4(M_{1A} + M_{3B} + M_{5A} + M_{7B} + \ldots) + 4(M_{1B} + M_{3A} + M_{5B} + M_{7A} + \ldots) + 8(M_{2A} + M_{4A} + M_{6A} + M_{8A} + \ldots) \quad (8)$$

generally, for $n \gg 2$

$$L_e(n) = L_e(n-1) + 4(M_{(2n-1)A} + M_{(2n-1)B} + M_{2nA} + M_{(2n+2)A}) \quad (9)$$

From the form of equation 8 it can be seen that when n is large, $L_e(n)$ attains a steady state limiting value. With the same provision it follows that $L_T(k)$ will assume the form of a block of initial terms with subsequent monotonic increases whose rate is determined by pole pitch.

Grover[260] gives expressions for evaluating self and mutual inductances. For L_1 and L_2, the standard expression used includes a term which allows for the finite section of the conductor. For M_1 and the subsequent mutuals, calculation is through either an expression such as given in Figure 2, or Grover's Q factor, which will give identical results.

Evaluation of the incremental term in equation 9, normalised by the pole pitch, reveals that

- colinear longitudinal filaments' normalised inductance varies as a function of n only,
- opposing longitudinal filaments' normalised inductance varies as n and width to pole pitch ratio only,
- transverse filaments' normalised inductance similarly varies only as n and width to pole pitch ratio.

A running summation of the incremental terms normalised by the pole pitch and k, will reach an asymptotic value, defined as L_a, such that

$$L_a = \frac{2}{k\lambda} \cdot 4 \sum_{n=0}^{k-1} (M_{(2n-1)A} + M_{(2n-1)B} + M_{2nA} + M_{(2n+2)A}) \quad (10)$$

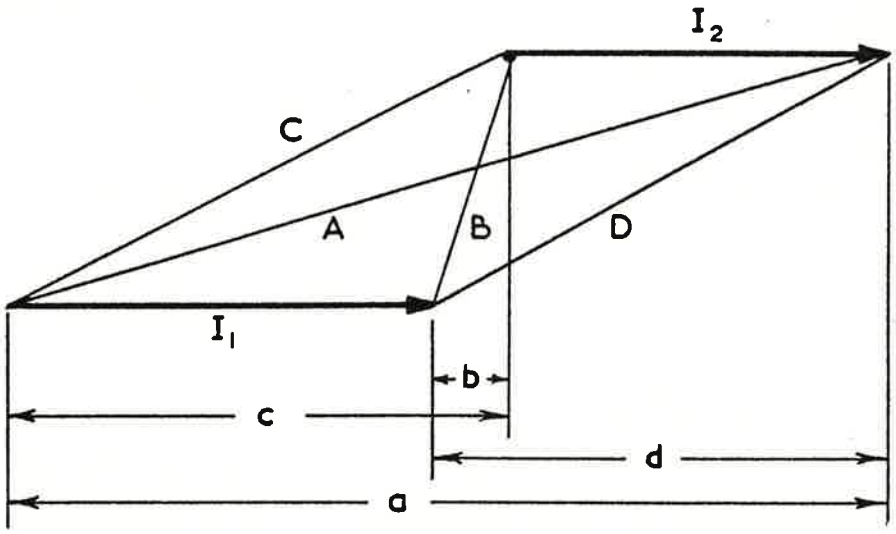

$$M = \frac{\mu_o}{4\pi} \left\{ \log_e \left[\frac{(A+a)^a (B+b)^b}{(C+c)^c (D+d)^d} \right] + C + D - A - B \right\}$$

Figure 2. Mutual inductance between parallel current elements.

Equation 2 can be rewritten as

$$L_T(k) = k\,L_e(0) + (k-1)\,(4M_{2A}) + \frac{k\lambda}{2}\,L_a$$

and since

$$k \simeq \frac{2G}{\lambda} \text{ and } L_e(0) = 2(L_1 + M_1) + L_2,$$
$$L_T(k) = \frac{2G}{\lambda}\,L_i + G\,L_a = G\,(\frac{2}{\lambda}\,L_i + L_a) \qquad (11)$$

where

$$L_i = 2(L_1 + M_1) + L_2 + 4M_{2A}$$

The strip self inductance L_G used in equation 1 and the main text is the same quantity as $L_T(k)$.

4. Mutual Inductance Structure

Mutual inductance calculation follows the same strategy as self inductance calculation. The parallel expression to equation 2 is given by

$$M_T(k) = \sum_{m=0}^{k} M_e(m) \qquad (12)$$

where $M_T(k)$ is the total mutual inductance between two phases of LSM, with k elements. The calculation can be performed for various relative phase displacements, and the main text explains how the remaining phase effects can be lumped together to refer to the first phase. Figure 1c shows the limb representation between a reference phase and a second double layer phase winding displaced by a fraction F of a wavelength.

Because of the intimate positioning of the limbs with low values of F, the initial inductance must include limbs up to m=2. However, the same structure emerges, with the final result

$$M_T(k) = M_G = G(\frac{2}{\lambda} M_i + M_a) \quad (13)$$

where M_i and M_a are the initial and asymptotic inductances respectively.

Figure 3 shows L_a and M_a for a range of width to pole pitch ratios. (L_a is invariably negative.)

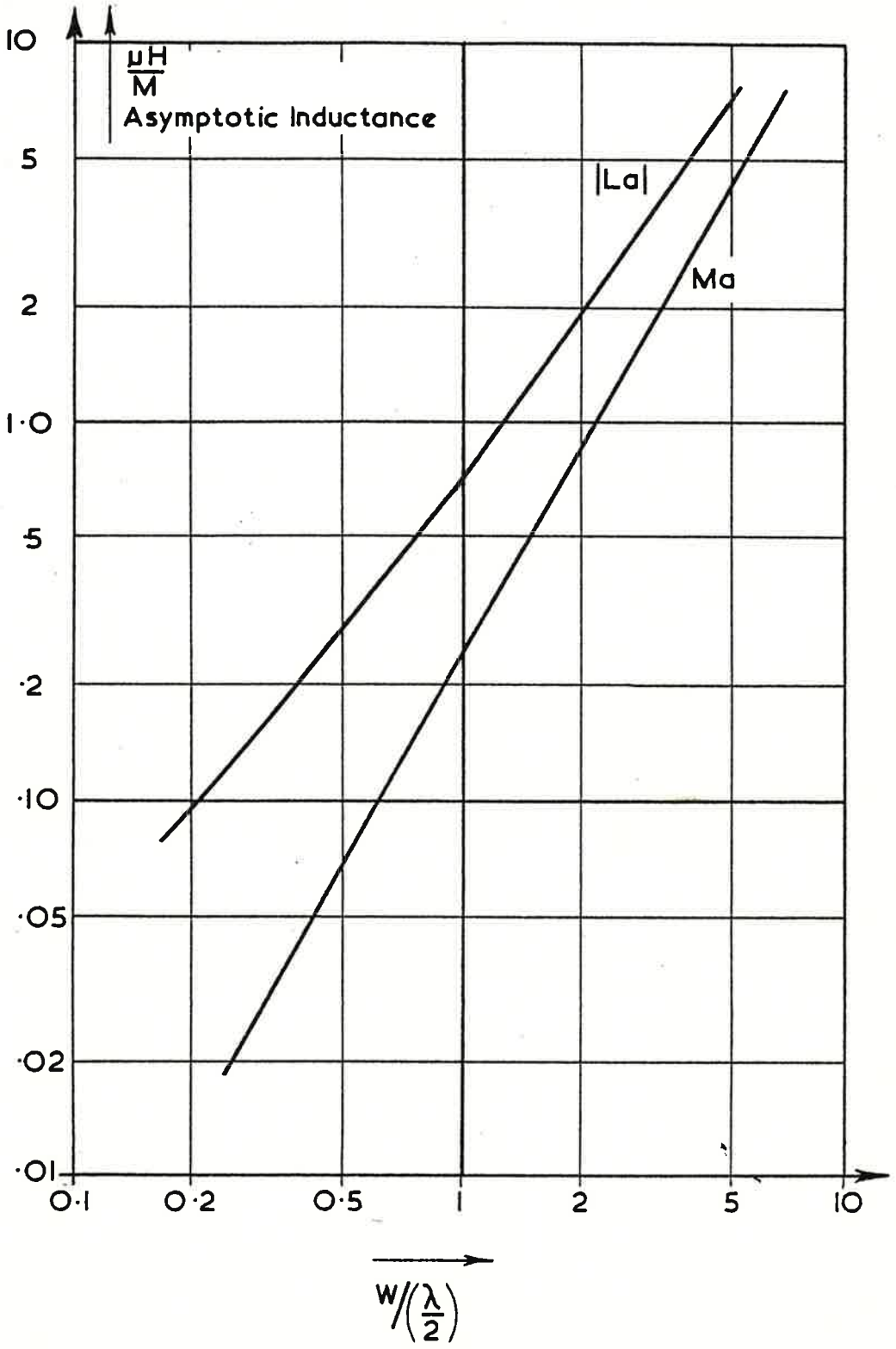

Figure 3. Asymptotic Self and Mutual Inductance as a function of width / pole pitch.

APPENDIX IV

FLUX LINKAGE AND INDUCED EMF IN AIR CORED MACHINES

(Reference 222)

TECHNICAL MEMORANDUM NO. 10

TITLE : FLUX LINKAGE AND INDUCED EMF IN AIR CORED MACHINES.

AUTHOR : E. ABEL

DATE : FEBRUARY 1976.
REVISED NOVEMBER 1978.

CONTENTS

Flux Linkage and Induced EMF in Air Cored Machines

1 INTRODUCTION

For the efficient design of air cored linear superconducting machinery it is necessary to be able to calculate accurately the emf induced in an armature phase winding by the superconducting magnets moving at a particular speed. If this value is known, for example, for a full pitched coil, conventional rotating machinery procedures can be used to establish the open circuit terminal phase voltage (the back emf). In this way the effects of short pitching, transposition and parallel and series interconnection of the individual conductor bars into a phase winding can also be calculated.

In common with machine practice, it is assumed that the machine is fed with balanced voltages or currents, and is operating in steady-state conditions. Phase inbalance can in fact be treated by using the concept of positive, zero and negative sequence currents, but will not be discussed further in this memorandum.

2 DERIVATION OF BACK EMF RELATIONSHIPS

2.1 Relationship with Rate of Change of Flux Linkage

The electromagnetic induction equation relates the emf e induced in a circuit which experiences a rate of change of flux linkage $\frac{d\phi}{dt}$.

$$e = - \frac{d\phi}{dt} \tag{1}$$

If the field winding is moving at a synchronous velocity v m/s, and the spatial variation of the flux linkage ϕ weber-turns is known for the field coil, then the temporal back emf e_B in the armature can be deduced from:

$$e_B = - \frac{d\phi}{dt}$$

$$= - \frac{d\phi}{dx} \cdot \frac{dx}{dt}$$

or

$$e_B = - v \cdot \frac{d\phi}{dx} \tag{2}$$

i.e., for balanced conditions, the temporal variation in back emf is proportional to the product of the synchronous velocity and the spatial variation of flux linkage.

2.2 Rate of Change of Flux Linkage

The rate of change of flux linkage may be calculated from knowledge of the vertical flux density at the track level produced by the superconducting coil.

Figure 1 shows a generalised current coil, with positive sensed current flowing. The vertical z axis is positioned so that it lies along the axial line of maximum field, normal to the coil plane. The x axis lies parallel to the direction of motion of the vehicle coil array. The track coils may be modelled as closed turns of full pitch, and for ease of calculation in this particular case are assumed to be symmetrical in the y plane, and parallel to the vehicle coil.

Consider a transverse strip of width dx located a distance x from the coil axis (Figure 1). The vertical flux density seen by the strip varies along its width in a manner determined by coil geometry dimensions, and current. The flux $d\phi$ linked by the strip is simply given by

$$d\phi = \left(\int_{-b}^{b} B_z \, dy\right) dx \qquad \text{weber-turns} \qquad (3)$$

$$\text{i.e.} \quad \frac{d\phi}{dx} = \int_{-b}^{b} B_z \, dy \qquad \text{weber-turns/metre} \qquad (4)$$

The effect of having the track coils offset is merely to alter the limits of integration. For the most common cases of tandem arranged vehicle coils the zero offset position links the most flux.

Note that expression (4) is valid whatever topology of coils is chosen, with whatever end winding geometry.

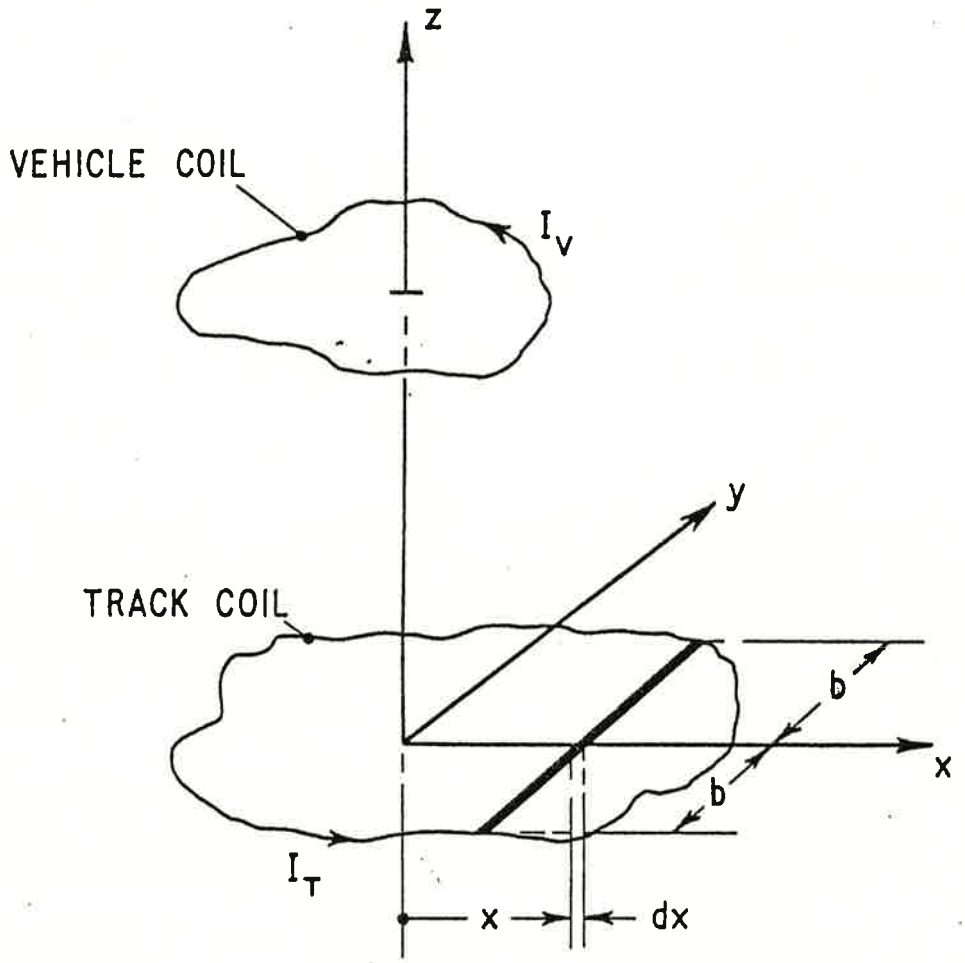

Figure 1. Generalized Vehicle and Track Coils.

2.3 The Effect of Neighbouring Coils

2.3.1 Dipole Approximation of Field

Because the LSM is air cored, the fields produced by vehicle coil arrays can be superposed. In effect it is not normally necessary to perform the calculation to include all vehicle coils, if the array is composed of a large number, as the effects of far-off coils become negligibly small. It is worth demonstrating this point with a simple example.

The external field of a current loop can be decomposed into an infinite series of multipoles. In the coil plane,

$$B(r) = \sum_{n=2}^{\infty} \frac{\mu_n}{r^{n+1}} \qquad (5)$$

μ_n is the nth pole magnetic moment, and r is the distance from the coil centre line to the field point considered.

Since only far-off effects are concerned, the higher orders can be neglected. The coil now appears as a dipole, and its field diminishes as the cube of the distance (twice the distance, one eigth the field, etc). For the case of incremental contributions of 2N neighbouring coils (with, for this example, alternating polarity) to the total field of the reference coil, on its centre line,

$$B_z = -\frac{2\mu_2}{\left(\frac{\lambda}{2}\right)^3} + \frac{2\mu_2}{\left(\frac{2\lambda}{2}\right)^3} - \frac{2\mu_2}{\left(\frac{3\lambda}{2}\right)^3} + \ldots \qquad (6)$$

where $\frac{\lambda}{2}$ is the pole pitch of the magnet array and μ_2 the dipole moment of the coils (assumed to be equal). Equation 6 can be generalised to

$$B_z = -\frac{2\mu_2}{\left(\frac{\lambda}{2}\right)^3} \sum_{n=1}^{N} \frac{(-1)^{n-1}}{n^3}, \quad n = 1, 2, 3, 4 \ldots \qquad (7)$$

When N is even, grouping together the terms in pairs reduces (7) to:

$$B_z = -\frac{2\mu_2}{\left(\frac{\lambda}{2}\right)^3} \sum_{n=1}^{N-1} \left(\frac{1}{n^3} - \frac{1}{(n+1)^3} \right), \quad n = 1, 3, 5 \ldots \qquad (8)$$

The first few terms of equation (8), under the summation, are shown in Table 1.

n	$\frac{1}{n^3} - \frac{1}{(n+1)^3}$
1	0.875
3	0.021412
5	0.003370
7	0.000962
9	0.000372
11	0.000173
13	0.000091
15	0.000052

TABLE 1 Initial Terms of Summation from Equation (8)

For an accuracy of better than 0.1% only 16 neighbouring coils (n=7, N=8) need be considered. Generally, roughly ten coils give an accuracy sufficient for most engineering design purposes.

2.3.2 Effect on Rate of Change of Flux Linkage

Figure 2 shows three coils from a typical alternating magnet array, with the rate of change of flux linkage $\frac{d\phi}{dx}$ of the reference coil A and the magnitudes of $\frac{d\phi}{dx}$ for neighbouring right and left hand coils within the half wavelength centred around A. Also shown is the total rate of change of flux linkage, which is forced to zero every $\frac{\lambda}{2}$ by conditions of symmetry.

The total effect of neighbouring coils on the value of rate of change of flux linkage for the range $0 < x < \frac{\lambda}{4}$ can be obtained as

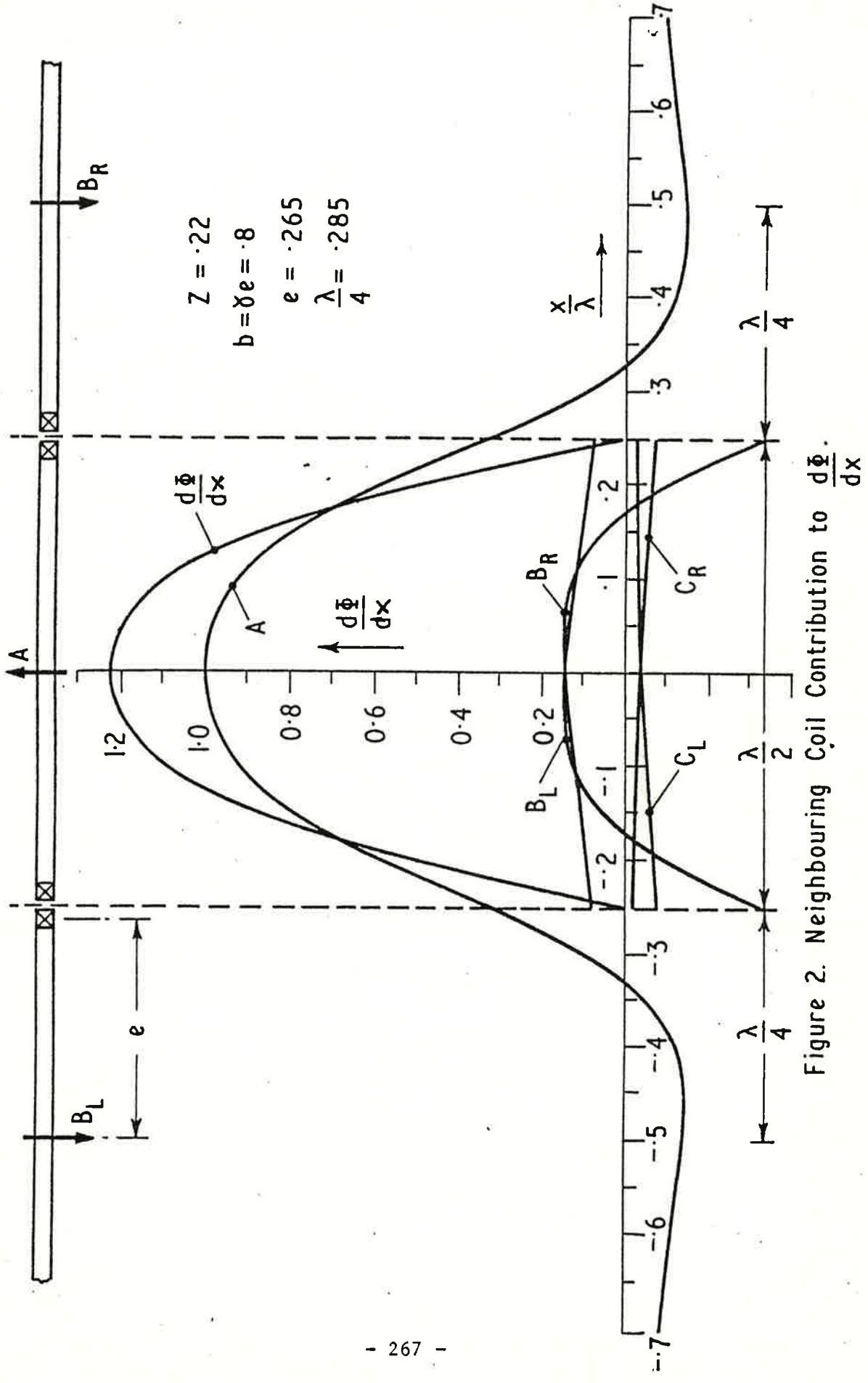

Figure 2. Neighbouring Coil Contribution to $\frac{d\Phi}{dx}$.

$$\frac{d\Phi}{dx} = \left.\frac{d\phi}{dx}\right|_x - \left.\frac{d\phi}{dx}\right|_{\frac{\lambda}{2}-x} - \left.\frac{d\phi}{dx}\right|_{\frac{\lambda}{2}+x} + \left.\frac{d\phi}{dx}\right|_{\lambda-x} + \left.\frac{d\phi}{dx}\right|_{\lambda+x}$$

$$A \qquad B_R \qquad B_L \qquad C_R \qquad C_L$$

$$- \left.\frac{d\phi}{dx}\right|_{\frac{3\lambda}{2}-x} - \left.\frac{d\phi}{dx}\right|_{\frac{3\lambda}{2}+x} + \left.\frac{d\phi}{dx}\right|_{2\lambda-x} + \left.\frac{d\phi}{dx}\right|_{2\lambda+x} - \ldots.$$

$$D_R \qquad D_L \qquad E_R \qquad E_L$$

$$\text{i.e.} \quad \frac{d\Phi}{dx} = \left.\frac{d\phi}{dx}\right|_x + \sum(-1)^n \left.\frac{d\phi}{dx}\right|_{\frac{n\lambda}{2}\pm x}, \quad n = 1, 2, 3 \ldots. \qquad (9)$$

For the optional designs involving only the same sensed magnets, (Magneplane, Wolfson 0.4 m pole pitch) n takes only even values in equation 9, and may be expressed as

$$\frac{d\Phi}{dx} = \left.\frac{d\phi}{dx}\right|_x + \sum \left.\frac{d\phi}{dx}\right|_{n\lambda\pm x}, \quad n = 1, 2, 3 \ldots \qquad (10)$$

3 RECTANGULAR COILS

3.1 Evaluation of $\frac{d\phi}{dx}$

Appendix I evaluates the rate of change of flux linkage with respect to the off axis track element as a function of coil half width and length, track half width, coil height and longitudinal off axis position.

$$\text{i.e.} \quad \frac{d\phi}{dx} = fn(\gamma e, e, b, z, x) \qquad (11)$$

Equation A-11 can be slightly simplified by considering the common design case $\gamma e = b$ (i.e. track width = coil width), and equation A-12 results. Both equations can be solved relatively easily using the substitutions (A-13 to A-15) which are:

$$E = \frac{e \pm x}{z} \tag{12}$$

$$R1 = \sqrt{\left(\frac{xe + b}{z}\right)^2 + E^2 + 1} \tag{13}$$

$$R2 = \sqrt{\left(\frac{xe - b}{z}\right)^2 + E^2 + 1} \tag{14}$$

so that, for a particular off axis position, x.

$$\frac{d\phi}{dx} \cdot \frac{10}{I} = \left[\frac{2E}{1+E^2}(R1 - R2) + \ln\left\{\frac{(R1 - E)(R2 + E)}{(R2 - E)(R1 + E)}\right\}\right]\Bigg|_{E = \frac{e+x}{z}} + \left[\frac{2E}{1+E^2}(R1 - R2) + \ln\left\{\frac{(R1 - E)(R2 + E)}{(R2 - E)(R1 + E)}\right\}\right]\Bigg|_{E = \frac{e-x}{z}} \tag{15}$$

The Appendix also shows the variation of (15) with x, and describes how to use the program.

3.2 Evaluation of $\frac{d\Phi}{dx}$

Equation (9) has shown how the successive neighbouring coils' $\frac{d\phi}{dx}$ contributes to the total $\frac{d\phi}{dx}$. For a particular coil, its effect within the range $0 < x < \frac{\lambda}{4}$ under the first coil can be found by incrementing or decreasing the $\frac{n\lambda}{2} \pm x$ term by the amount $\frac{\lambda}{4q}$, where q is the number of divisions of $\frac{\lambda}{4}$ chosen for harmonic analysis. Having done this for each successive coil, the following array is obtained.

A	B_R	B_L	C_R	C_L
0		$\frac{\lambda}{2}$		λ
$\frac{\lambda}{4}\cdot q$	$\frac{\lambda}{4}\ \frac{(2q-1)}{q}$	$\frac{\lambda}{4}\ \frac{(2q+1)}{q}$	$\frac{\lambda}{4}\ \frac{(4q-1)}{q}$	$\frac{\lambda}{4}\ \frac{(4q+1)}{q}$
$\frac{\lambda}{4}\ \frac{(q-1)}{q}$	$\frac{\lambda}{4}\ \frac{(q+1)}{q}$	$\frac{\lambda}{4}\ \frac{(3q-1)}{q}$	$\frac{\lambda}{4}\ \frac{(3q+1)}{q}$	$\frac{\lambda}{4}\ \frac{(5q-1)}{q}$
$\frac{\lambda}{4}$		$\frac{3\lambda}{4}$		$\frac{5\lambda}{4}$

TABLE 2 Values of x to be used in Program to evaluate (9)

The number of rows is simply q+1 and the number of columns is the total number of coils included. It is worthwhile evaluating the first row and finding the point where an incremental pair of coils alter $\left.\frac{d\Phi}{dx}\right|_x$ by, say, less than 1%, and using this as the value for the numbers of columns for subsequent rows.

When the $\frac{d\phi}{dx}$ values obtained using Table 2 are summated as in (9) (taking into account the coil polarities) then the total flux linked by the elemental strip dx is found, being a one dimensional array of size q+1.

Figure 3 shows the effect on $\frac{d\Phi}{dx}$ of including neighbouring coils. Because the case considered is for an alternating array, the successive points alternate about the final value. Also shown is a more rapid convergence, using the incremental difference of successive coil pairs. For this particular case, only ten neighbouring coils (i.e. five on either side of the first coil) need to be considered to give a reasonable result. Note also the way in which the $x = \frac{\lambda}{4}$ value is rapidly forced to zero by the symmetry of the coil array.

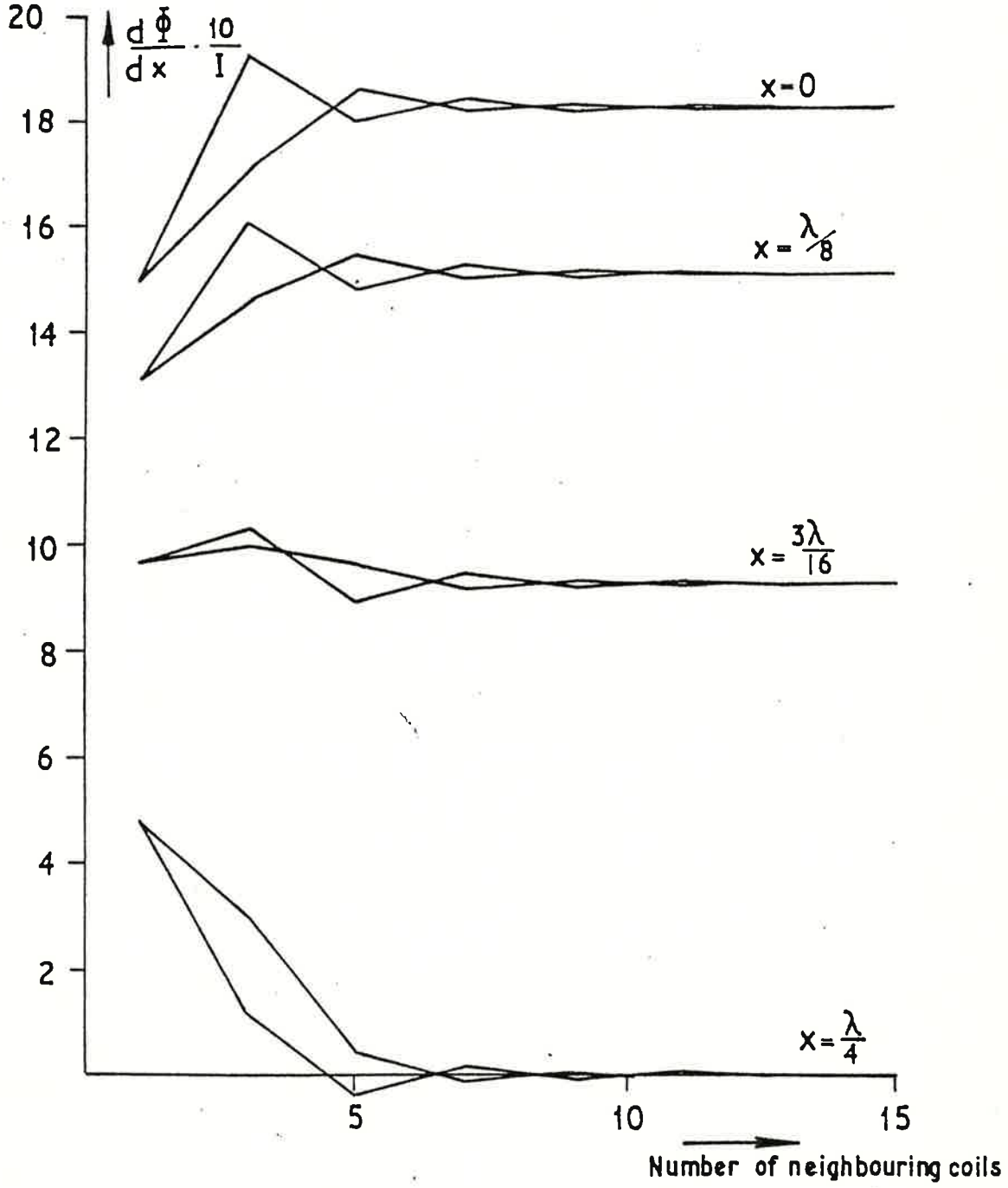

Figure 3. Effect of neighbouring coils on rate of change of flux.

The parameter values used for the figures for rectangular coils are given in Table 3.

Vehicle coil half length	e	0.265
Vechicle coil half width	γe	0.8
Vehicle to track seperation	z	0.22
Track half width	b	0.8
Quarter Wavelength	λ/4	0.285

TABLE 3 Rectangular Coil Parameters

3.3 Harmonics in the Air Gap Flux Linkage

Once the total rate of change of air gap flux linkage with the full pitch track coils is known, its harmonic make-up can be evaluated. If $\frac{d\Phi}{dx}$ is evaluated at x = q+1 positions in the quarter wavelength (note x = λ/4, $\frac{d\Phi}{dx}$ = 0) the Fourier coefficients can be found for the first 2q+1 harmonics. With the conventions used, x = o for maximum linkage and x = $\frac{\lambda}{4}$ for zero linkage for the elemental strip, so only odd harmonics will be present in a cosinusoidal summation. For a fuller treatment of harmonic analysis, refer to TM 13, Fourier Analysis of Linear Machine Airgap Fluxes.

4 CIRCULAR AND RACETRACK COILS

The field variation at off axis positions for circular coils involves solution of complete elliptical integrals of the first and second kind. Racetrack off axis positions involve combinations of straight line element type formulae, with extra terms involving solution of incomplete elliptical integrals of the first and second kind. The overall technique for solution of rate of change of air gap flux linkage is similar to that used for rectangular coils, but is computationally more awkward. When working at large airgaps, an equivalent area rectangular coil can be used for first order approximation, with only a slight loss of accuracy.

5 CONCLUSIONS

The way in which the rate of change of flux linkage between a track coil and an array of vehicle magnets varies has been demonstrated, with particular reference to rectangular coils. From this, the temporal variation of induced emf in the air cored machine can be directly computed, complete with harmonic content, and so the vehicle force profile with any pulsations present can be established.

1st Draft: February 1976
Revised: November 1978

APPENDIX I - RATE OF CHANGE OF FLUX LINKAGE FOR A RECTANGULAR COIL

1 Flux Density Under a Rectangular Coil

Using the Biot-Savart relationship, the field for a finite length straight conductor can be found. For a rectangular coil with sides 2e, and 2γe (Figure A-1) the vertical field at a point (x, y) can be found by superposition of the field from the four sides to be given by

$$
\begin{aligned}
B_z = \frac{\mu I}{4\pi} & \frac{e+x}{(e+x)^2+z^2}\left(\frac{\gamma e+y}{\left[(e+x)^2+(\gamma e+y)^2+z^2\right]^{1/2}} + \frac{\gamma e-y}{\left[(e+x)^2+(\gamma e-y)^2+z^2\right]^{1/2}}\right) \\
+ & \frac{e-x}{(e-x)^2+z^2}\left(\frac{\gamma e+y}{\left[(e-x)^2+(\gamma e+y)^2+z^2\right]^{1/2}} + \frac{\gamma e-y}{\left[(e-x)^2+(\gamma e-y)^2+z^2\right]^{1/2}}\right) \\
+ & \frac{\gamma e+y}{(\gamma e+y)^2+z^2}\left(\frac{e+x}{\left[(e+x)^2+(\gamma e+y)^2+z^2\right]^{1/2}} + \frac{e-x}{\left[(e-x)^2+(\gamma e+y)^2+z^2\right]^{1/2}}\right) \\
+ & \frac{\gamma e-y}{(\gamma e-y)^2+z^2}\left(\frac{e+x}{\left[(e+x)^2+(\gamma e-y)^2+z^2\right]^{1/2}} + \frac{e-x}{\left[(e-x)^2+(\gamma e+y)^2+z^2\right]^{1/2}}\right)
\end{aligned}
\qquad \text{(A-1)}
$$

Integration of expression A-1 is tedions, but is eased by similarities throughout the terms. Re-writing A-1, replacing the terms sequentially,

$$B_z = \frac{\mu I}{4\pi}\left[(A + B) + (C + D) + (E + F) + (G + H)\right] \qquad \text{(A-2)}$$

2 Evaluation of $\int_{-b}^{b} B_z \, dy$

Taking the terms in the square brackets of A-2,

$$\int_{-b}^{b} A\,dy = \frac{e+x}{\left[(e+x)^2 + z^2\right]} \int_{-b}^{b} \frac{(\gamma e + y)\,dy}{\left[(e+x)^2 + (\gamma e+y)^2 + z^2\right]^{\frac{1}{2}}} \tag{A-2}$$

$$= \frac{e+x}{(e+x)^2 + z^2}\left[\left[(e+x)^2 + (\gamma e+b)^2 + z^2\right]^{\frac{1}{2}} - \left[(e+x)^2 + (\gamma e-b) + z^2\right]^{\frac{1}{2}}\right] \tag{A-3}$$

It is found that similarly, $\int_{-b}^{b} B\,dy = \int_{-b}^{b} A\,dy$ (A-4)

Also

$\int_{-b}^{b} C\,dy$ and $\int_{-b}^{b} D\,dy$ are merely the previous expressions with $-x$ replacing x which does not affect the integration.

So

$\int_{-b}^{b} C\,dy = \int_{-b}^{b} D\,dy$, and normalizing by z^2

$$= \frac{e-x}{\left(\frac{e-x}{z}\right)^2 + 1}\left[\left[\left(\frac{\gamma e+b}{z}\right)^2 + \left(\frac{e-x}{z}\right)^2 + 1\right]^{\frac{1}{2}} - \left[\left(\frac{\gamma e-b}{z}\right)^2 + \left(\frac{e-x}{z}\right)^2 + 1\right]^{\frac{1}{2}}\right] \tag{A-5}$$

$$\int_{-b}^{b} E\,dy = e+x \int_{-b}^{b} \frac{(\gamma e + y)\,dy}{\left((\gamma e+y)^2 + z^2\right)\left((e+x)^2 + (\gamma e+y)^2 + z^2\right)^{\frac{1}{2}}} \tag{A-6}$$

using the substitution

$$t^2 = (\gamma e + y)^2 + (e + x)^2 + z^2$$

then $2t\,dt = 2(\gamma e + y)\,dy$

and t_u = upper limit $= \left[(\gamma e + b)^2 + (e + x)^2 + z^2\right]^{\frac{1}{2}}$

t_l = lower limit $= \left[(\lambda e - b)^2 + (e + x)^2 + z^2\right]^{\frac{1}{2}}$

So

$$\int_{-b}^{b} E\,dy = e + x \int_{t_l}^{t_u} \frac{dt}{(t^2 - (e + x)^2)}$$

since in the denominator the coefficient of t^2 is unity, i.e. > 0, and also $-(e + x)^2 < 0$,

$$\int_{-b}^{b} E\,dy = \frac{1}{2\sqrt{(e + x)^2}} \ln \left\{ \frac{t\sqrt{1} - \sqrt{(e+x)^2}}{t\sqrt{1} + \sqrt{(e+x)^2}} \right\} \Bigg|_{t_l}^{t_u} = \tfrac{1}{2} \ln \frac{t - (e+x)}{t + (e+x)} \Bigg|_{t_l}^{t_u}$$

So

$$\int_{-b}^{b} E\,dy = \tfrac{1}{2} \ln \frac{t_u - (e+x)}{t_L - (e+x)} - \tfrac{1}{2} \ln \frac{t_u + (e+x)}{t_L + (e+x)}$$

$$= \frac{1}{2} \ln \left\{ \frac{\left[\left(\frac{\gamma e + b}{z}\right)^2 + \left(\frac{e+x}{z}\right)^2 + 1 \right]^{1/2} - \left(\frac{e+x}{z}\right)}{\left[\left(\frac{\gamma e - b}{z}\right)^2 + \left(\frac{e+x}{z}\right)^2 + 1 \right]^{1/2} - \left(\frac{e+x}{z}\right)} \right\} - \frac{1}{2} \ln \left\{ \frac{\left[\left(\frac{\gamma e + b}{z}\right)^2 + \left(\frac{e+x}{z}\right)^2 + 1 \right]^{1/2} + \left(\frac{e+x}{z}\right)}{\left[\left(\frac{\gamma e - b}{z}\right)^2 + \left(\frac{e+x}{z}\right)^2 + 1 \right]^{1/2} + \left(\frac{e+x}{z}\right)} \right\}$$

(A-7)

As with $\int B$ and $\int A$, the change of sign for y effects the limits and term signs of $\int G$, which evaluate as equivalent to $\int E$

$$\text{i.e.} \quad \int_{-b}^{b} G\, dy = \int_{-b}^{b} E\, dy \qquad \text{(A-8)}$$

Also as with C and D, F and H are the same as E and G, with x replaced by $-x$, so

$$\int_{-b}^{b} F\, dy = \int_{-b}^{b} H\, dy$$

$$= \frac{1}{2} \ln\left\{\frac{\left[\left(\frac{\gamma e+b}{z}\right)^2 + \left(\frac{e-x}{z}\right)^2 + 1\right]^{1/2} - \left(\frac{e-x}{z}\right)}{\left[\left(\frac{\gamma e-b}{z}\right)^2 + \left(\frac{e-x}{z}\right)^2 + 1\right]^{1/2} - \left(\frac{e-x}{z}\right)}\right\} - \frac{1}{2} \ln\left\{\frac{\left[\left(\frac{\gamma e+b}{z}\right)^2 + \left(\frac{e-x}{z}\right)^2 + 1\right]^{1/2} + \left(\frac{e-x}{z}\right)}{\left[\left(\frac{\gamma e-b}{z}\right)^2 + \left(\frac{e-x}{z}\right)^2 + 1\right]^{1/2} + \left(\frac{e-x}{z}\right)}\right\}$$

(A-9)

3 Rate of Change of Flux Linkage

The flux linkage $d\phi$ of an element of track dx, x from the centre of the field coil axis, is simply

$$d\phi = \left(\int_{-b}^{b} B_z\, dy\right) dx \qquad \text{(A-10)}$$

where the vertical field component B_z at the track surface is considered between the track coil width $2b$.

Using expression A-2 through to A-10, the rate of change of flux linkage, $d\phi/dx$ is given by

$$\frac{d\phi}{dx} = \frac{4\pi\ 10^{-7}\ I\ 10^{6}}{4\pi}\left[\int_{-b}^{b} (A + B + C + D + E + F + G + H)\, dy\right] \text{ weber-turns per metre}$$

where I is the field coil current in MAT.

i.e.

$$\frac{d\phi}{dx} = \frac{I}{10}\left[\frac{2\,\frac{e+x}{z}}{\left(\frac{e+x}{z}\right)^2+1}\left(\sqrt{\left(\frac{\gamma e+b}{z}\right)^2+\left(\frac{e+x}{z}\right)^2+1}-\sqrt{\left(\frac{\gamma e-b}{z}\right)^2+\left(\frac{e+x}{z}\right)+1}\right)\right.$$

$$+\ln\left\{\frac{\sqrt{\left(\frac{\gamma e+b}{z}\right)^2+\left(\frac{e+x}{z}\right)^2+1}-\frac{e+x}{z}}{\sqrt{\left(\frac{\gamma e-b}{z}\right)^2+\left(\frac{e+x}{z}\right)^2+1}-\frac{e+x}{z}}\right\}-\ln\left\{\frac{\sqrt{\left(\frac{\gamma e+b}{z}\right)^2+\left(\frac{e+x}{z}\right)^2+1}+\frac{e+x}{z}}{\sqrt{\left(\frac{\gamma e-b}{z}\right)^2+\left(\frac{e+x}{z}\right)^2+1}+\frac{e+x}{z}}\right\}$$

$$+\frac{2\,\frac{e-x}{z}}{\left(\frac{e-x}{z}\right)^2+1}\left(\sqrt{\left(\frac{\gamma e+b}{z}\right)^2+\left(\frac{e-x}{z}\right)^2+1}-\sqrt{\left(\frac{\gamma e-b}{z}\right)^2+\left(\frac{e-x}{z}\right)^2+1}\right)$$

$$\left.+\ln\left\{\frac{\sqrt{\left(\frac{\gamma e+b}{z}\right)^2+\left(\frac{e-x}{z}\right)^2+1}-\frac{e-x}{z}}{\sqrt{\left(\frac{\gamma e-b}{z}\right)^2+\left(\frac{e-x}{z}\right)^2+1}-\frac{e-x}{z}}\right\}-\ln\left\{\frac{\sqrt{\left(\frac{\gamma e+b}{z}\right)^2+\left(\frac{e-x}{z}\right)^2+1}+\frac{e-x}{z}}{\sqrt{\left(\frac{\gamma e-b}{z}\right)^2+\left(\frac{e-x}{z}\right)+1}+\frac{e-x}{z}}\right\}\right] \qquad \text{(A-11)}$$

For the case when the coil width ($2\gamma e$) equals the track armature width ($2b$) A-11 becomes

$$\frac{d\phi}{dx} = \frac{I}{10}\left[\frac{2\,\frac{e+x}{z}}{\left(\frac{e+x}{z}\right)^2+1}\left(\sqrt{\left(\frac{2b}{z}\right)^2+\left(\frac{e+x}{z}\right)^2+1}-\sqrt{\left(\frac{e+x}{z}\right)^2+1}\right)\right.$$

$$+\ln\left\{\frac{\sqrt{\left(\frac{2b}{z}\right)^2+\left(\frac{e+x}{z}\right)^2+1}-\frac{e+x}{z}}{\sqrt{\left(\frac{e+x}{z}\right)^2+1}-\frac{e+x}{z}}\right\}-\ln\left\{\frac{\sqrt{\left(\frac{2b}{z}\right)^2+\left(\frac{e+x}{z}\right)^2+1}+\frac{e+x}{z}}{\sqrt{\left(\frac{e+x}{z}\right)^2+1}+\frac{e+x}{z}}\right\}$$

$$+\frac{2\,\frac{e-x}{z}}{\left(\frac{e-x}{z}\right)^2+1}\left(\sqrt{\left(\frac{2b}{z}\right)^2+\left(\frac{e-x}{z}\right)^2+1}-\sqrt{\left(\frac{e-x}{z}\right)^2+1}\right)$$

$$\left.+\ln\left\{\frac{\sqrt{\left(\frac{2b}{z}\right)^2+\left(\frac{e-x}{z}\right)^2+1}-\frac{e-x}{z}}{\sqrt{\left(\frac{e-x}{z}\right)^2+1}-\frac{e-x}{z}}\right\}-\ln\left\{\frac{\sqrt{\left(\frac{2b}{z}\right)^2+\left(\frac{e-x}{z}\right)^2+1}+\frac{e-x}{z}}{\sqrt{\left(\frac{e-x}{z}\right)^2+1}+\frac{e-x}{z}}\right\}\right] \qquad \text{(A-12)}$$

both A-11 and A-12 can be solved fairly easily using the HP 9100 A calculator.

4 Solution of Equation A-10

Observing the form of equation A-11 it is apparent that the last three terms are simply the first three terms with $\frac{e+x}{z}$ replacing $\frac{e+x}{z}$. Further more the first three terms are composed of combinations of two square roots, and $\frac{e+x}{z}$.

Substituting

$$E = \frac{e \pm x}{z} \qquad \begin{matrix}(+\text{ve for 1st 3 terms} \\ -\text{ve for 2nd 3 terms})\end{matrix} \qquad \text{(A-13)}$$

$$R1 = \sqrt{\left(\frac{\gamma e + b}{z}\right)^2 + E^2 + 1} \qquad \text{(A-14)}$$

$$R2 = \sqrt{\left(\frac{\gamma e - b}{z}\right)^2 + E^2 + 1} \qquad \text{(A-15)}$$

A-11 becomes, therefore

$$\frac{d\phi}{dx} \cdot \frac{10}{I} = \left[\frac{2E}{1 + E^2}(R1 - R2) + \ln\left(\frac{(R1 - E)\ (R2 + E)}{(R2 - E)\ (R1 + E)}\right)\right]\Bigg|_{E = \frac{e+x}{z}}$$

$$+ \left[\frac{2E}{1 + E^2}(R1 - R2) + \ln\left(\frac{(R1 - E)\ (R2 + E)}{(R2 - E)\ (R1 + e)}\right)\right]\Bigg|_{E = \frac{e-x}{z}} \qquad \text{(A-16)}$$

The programme steps to evaluate A-16 are shown in Figures A-2 - 3, with annotated listings in Figures A-4 - 5, and are available for use on magnetic card. To use the card, load side one, start the programme, load z, γe and b, and run the programme. The values of

$$1 + \left(\frac{\gamma e \pm b}{z}\right)^2$$

are given in the y and z registers at step 19. The second side of the card is loaded, and the two previous values are loaded in registers d and c respectively. Values of e and z are written in steps 02 - 05 and 07 - 0b respectively. The value of x for which A-16 is required is loaded into the y register, and the programme is started.

The next few steps (68 - 7c) are for use in evaluating the effect of neighbouring coils on a strip confined to $0 < x < \frac{\lambda}{4}$ under the first coil,

and is discussed in section 3.2 of the main text.

The plotter options are used to provide graphical displays of $\frac{d\phi}{dx}$, and have to be wiitten over the steps used for printing. The step size in x is entered in 77 - 79 or 78 - 7a, and whether this is added or subtracted from initial x, in step 01 or 00. Horizontal scaling sets x times 5000, i.e. 2.5 x per mm. Vertical scaling is 200 times the $\frac{d\phi}{dx} \cdot \frac{10}{I}$ value, i.e. 0.1 $\frac{d\phi}{dx} \cdot \frac{10}{I}$ per mm. Both can be changed by over-writing steps 69 - 71 or 6a - 72, if required.

The second option allows the $\frac{d\phi}{dx} \cdot \frac{10}{I}$ term (F) to be negated, but this requires a manual continue to be used after step 7d. This option was used to plot Figure 2 of the main text.

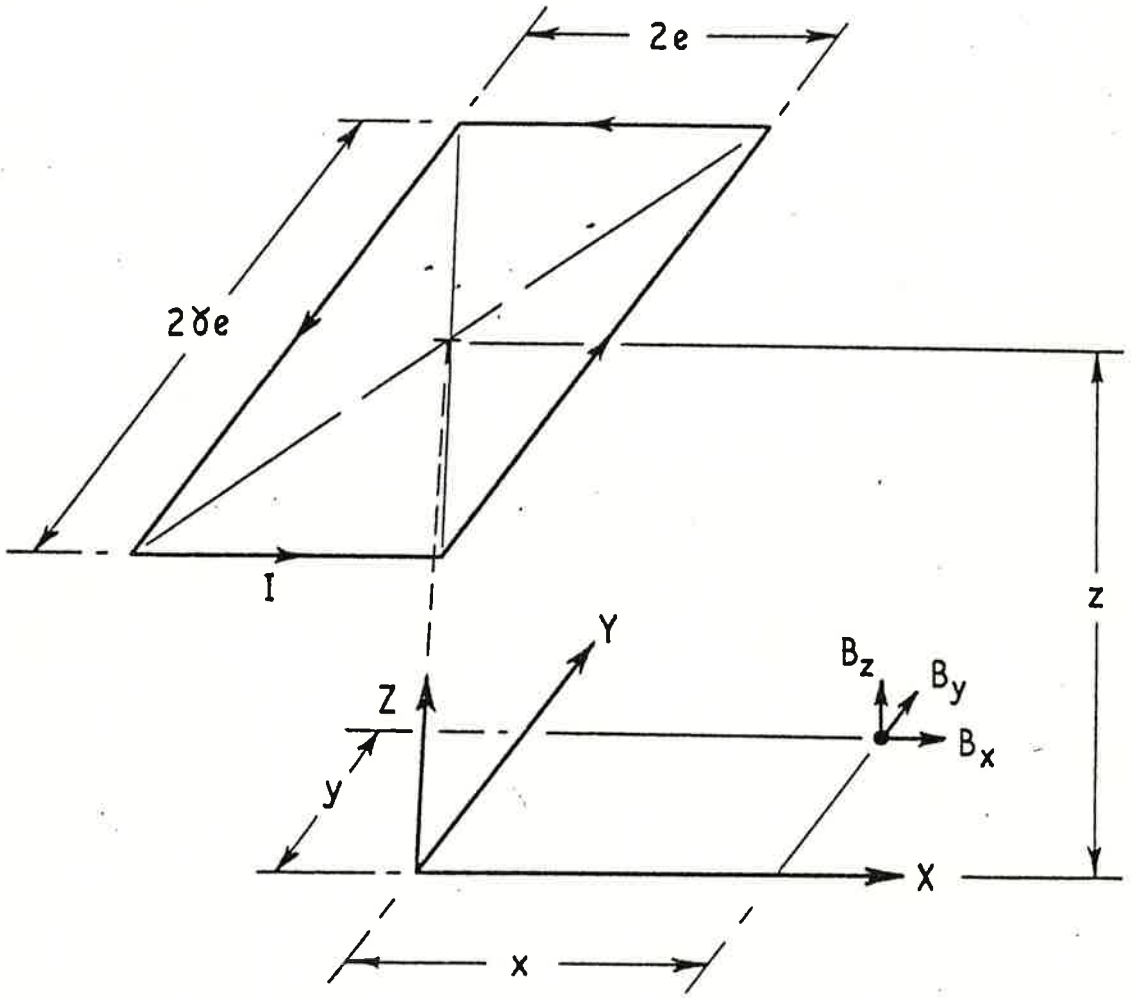

Figure A-1. Field Conventions Adopted for Rectangular Coils.

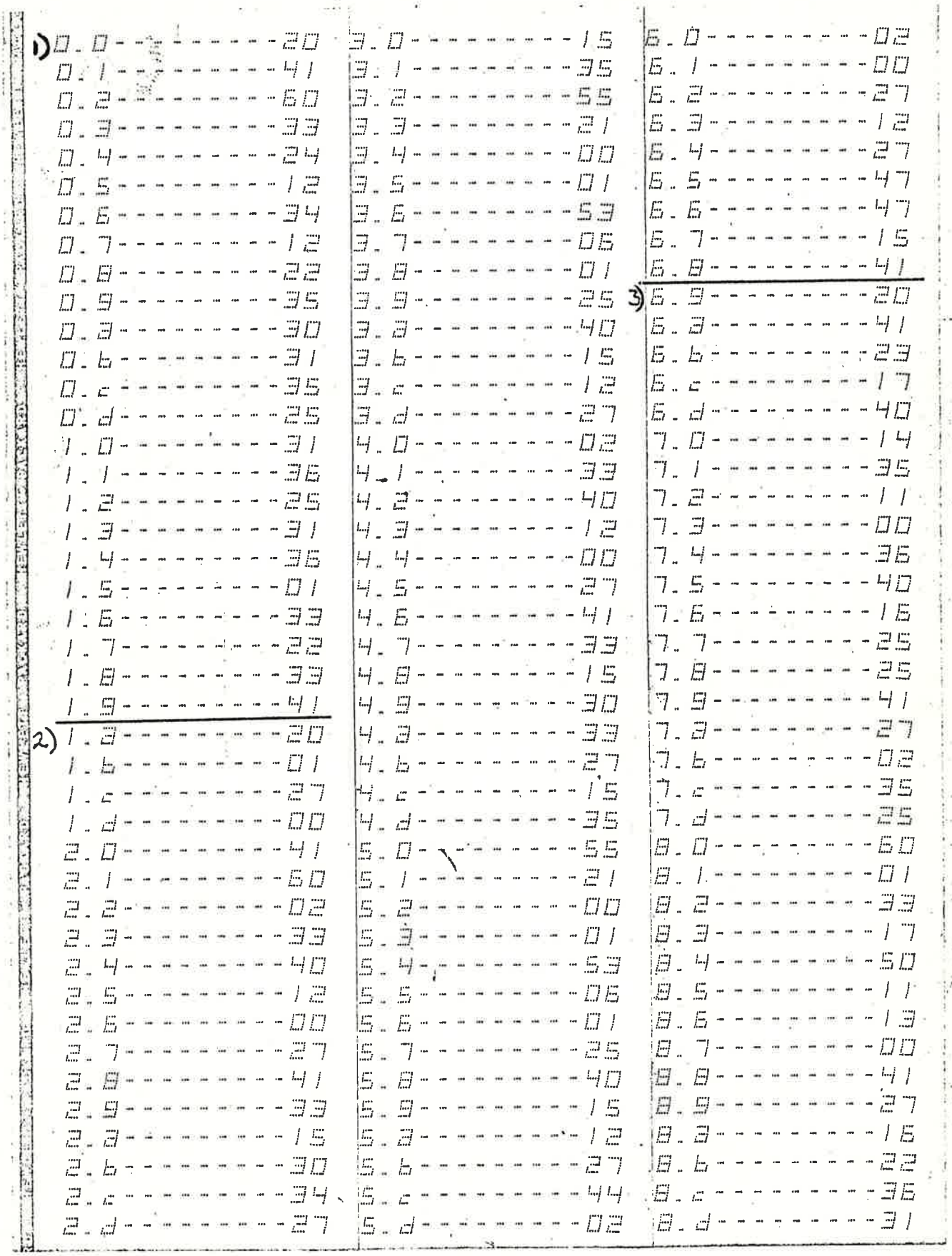

FIGURE A-2 (1) Input values for side two (2) $\frac{d\Phi}{dx}$ (3) Fourier coefficients

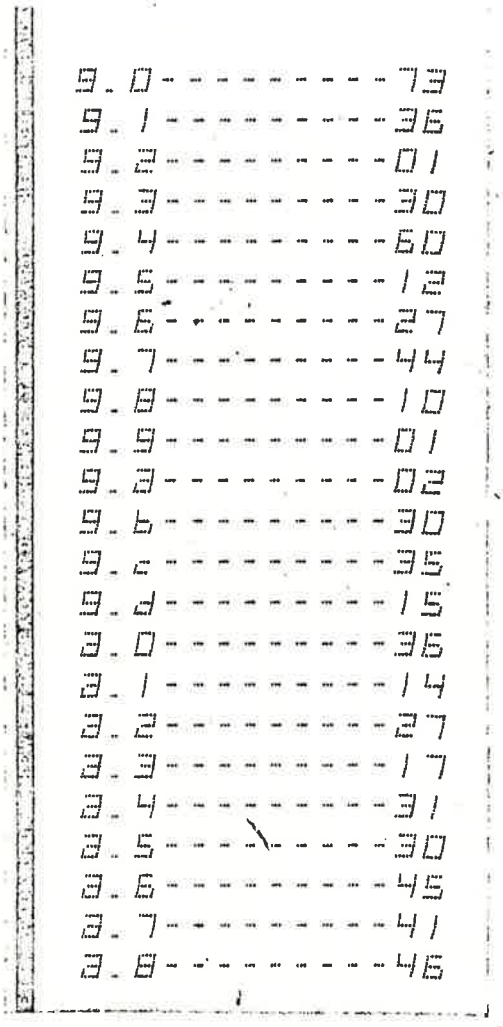

Figure A-2 continued

0.0 - - - - - - - - - 40	3.0 - - - - - - - - - 40	6.0 - - - - - - - - - 10
0.1 - - - - - - - - - 11	3.1 - - - - - - - - - 15	6.1 - - - - - - - - - 33
0.2 - - - - - - - - - 47	3.2 - - - - - - - - - 14	6.2 - - - - - - - - - 25
0.3 - - - - - - - - - 47	3.3 - - - - - - - - - 27	6.3 - - - - - - - - - 24
0.4 - - - - - - - - - 47	3.4 - - - - - - - - - 12	6.4 - - - - - - - - - 11
0.5 - - - - - - - - - 47	3.5 - - - - - - - - - 34	6.5 - - - - - - - - - 30
0.6 - - - - - - - - - 33	3.6 - - - - - - - - - 27	6.6 - - - - - - - - - 32
0.7 - - - - - - - - - 47	3.7 - - - - - - - - - 13	6.7 - - - - - - - - - 45
0.8 - - - - - - - - - 47	3.8 - - - - - - - - - 30	6.8 - - - - - - - - - 27
0.9 - - - - - - - - - 47	3.9 - - - - - - - - - 34	6.9 - - - - - - - - - 47
0.a - - - - - - - - - 47	3.a - - - - - - - - - 31	6.a - - - - - - - - - 47
0.b - - - - - - - - - 35	3.b - - - - - - - - - 35	6.b - - - - - - - - - 47
0.c - - - - - - - - - 40	3.c - - - - - - - - - 13	6.c - - - - - - - - - 47
0.d - - - - - - - - - 12	3.d - - - - - - - - - 22	6.d - - - - - - - - - 47
1.0 - - - - - - - - - 12	4.0 - - - - - - - - - 33	7.0 - - - - - - - - - 47
1.1 - - - - - - - - - 36	4.1 - - - - - - - - - 31	7.1 - - - - - - - - - 47
1.2 - - - - - - - - - 27	4.2 - - - - - - - - - 36	7.2 - - - - - - - - - 33
1.3 - - - - - - - - - 36	4.3 - - - - - - - - - 14	7.3 - - - - - - - - - 47
1.4 - - - - - - - - - 16	4.4 - - - - - - - - - 22	7.4 - - - - - - - - - 47
1.5 - - - - - - - - - 33	4.5 - - - - - - - - - 33	7.5 - - - - - - - - - 47
1.6 - - - - - - - - - 25	4.6 - - - - - - - - - 25	7.6 - - - - - - - - - 47
1.7 - - - - - - - - - 76	4.7 - - - - - - - - - 35	7.7 - - - - - - - - - 47
1.8 - - - - - - - - - 23	4.8 - - - - - - - - - 15	7.8 - - - - - - - - - 47
1.9 - - - - - - - - - 13	4.9 - - - - - - - - - 30	7.9 - - - - - - - - - 53
1.a - - - - - - - - - 17	4.a - - - - - - - - - 65	7.a - - - - - - - - - 00
1.b - - - - - - - - - 33	4.b - - - - - - - - - 33	7.b - - - - - - - - - 00
1.c - - - - - - - - - 26	4.c - - - - - - - - - 43	7.c - - - - - - - - - 46
1.d - - - - - - - - - 76	4.d - - - - - - - - - 05	
2.0 - - - - - - - - - 23	5.0 - - - - - - - - - 16	
2.1 - - - - - - - - - 14	5.1 - - - - - - - - - 54	
2.2 - - - - - - - - - 27	5.2 - - - - - - - - - 40	
2.3 - - - - - - - - - 13	5.3 - - - - - - - - - 10	
2.4 - - - - - - - - - 34	5.4 - - - - - - - - - 24	
2.5 - - - - - - - - - 12	5.5 - - - - - - - - - 11	
2.6 - - - - - - - - - 36	5.6 - - - - - - - - - 32	
2.7 - - - - - - - - - 02	5.7 - - - - - - - - - 01	
2.8 - - - - - - - - - 36	5.8 - - - - - - - - - 36	
2.9 - - - - - - - - - 01	5.9 - - - - - - - - - 44	
2.a - - - - - - - - - 22	5.a - - - - - - - - - 00	
2.b - - - - - - - - - 33	5.b - - - - - - - - - 00	
2.c - - - - - - - - - 25	5.c - - - - - - - - - 25	
2.d - - - - - - - - - 35	5.d - - - - - - - - - 24	

FIGURE A-3 Evaluation of $\frac{d\phi}{dx} \cdot \frac{10}{I}\Big|_x$ for Rectangular Coils

```
6.7----------27
6.8----------31
6.9----------02
6.a----------00
6.b----------00
6.c----------36
6.d----------05
7.0----------26
7.1----------03
7.2----------22
7.3----------36
7.4----------31
7.5----------42
7.6----------25
7.7----------21
7.8----------47
7.9----------47
7.a----------22
7.b----------44
7.c----------00
7.d----------00

0.0----------30
0.1----------33
0.2----------40
0.3----------11
0.4----------47
0.5----------47
0.6----------47
0.7----------33
0.8----------47
0.9----------47
0.a----------47
0.b----------35

5.b----------02
```

```
6.7----------27
6.8----------31
6.9----------32
6.a----------02
6.b----------00
6.c----------00
6.d----------36
7.0----------05
7.1----------26
7.2----------03
7.3----------22
7.4----------36
7.5----------31
7.6----------42
7.7----------25
7.8----------21
7.9----------47
7.a----------47
7.b----------22
7.c----------30
7.d----------46

0.0----------33
0.1----------40
0.2----------11
0.3----------47
0.4----------47
0.5----------47
0.6----------33

5.b----------01
```

FIGURE A-3 Continued

1) Evaluates input for side 2. 2) Evaluates coil array $\frac{d\Phi}{dx}$ 3) Evaluates Fourier coeffic

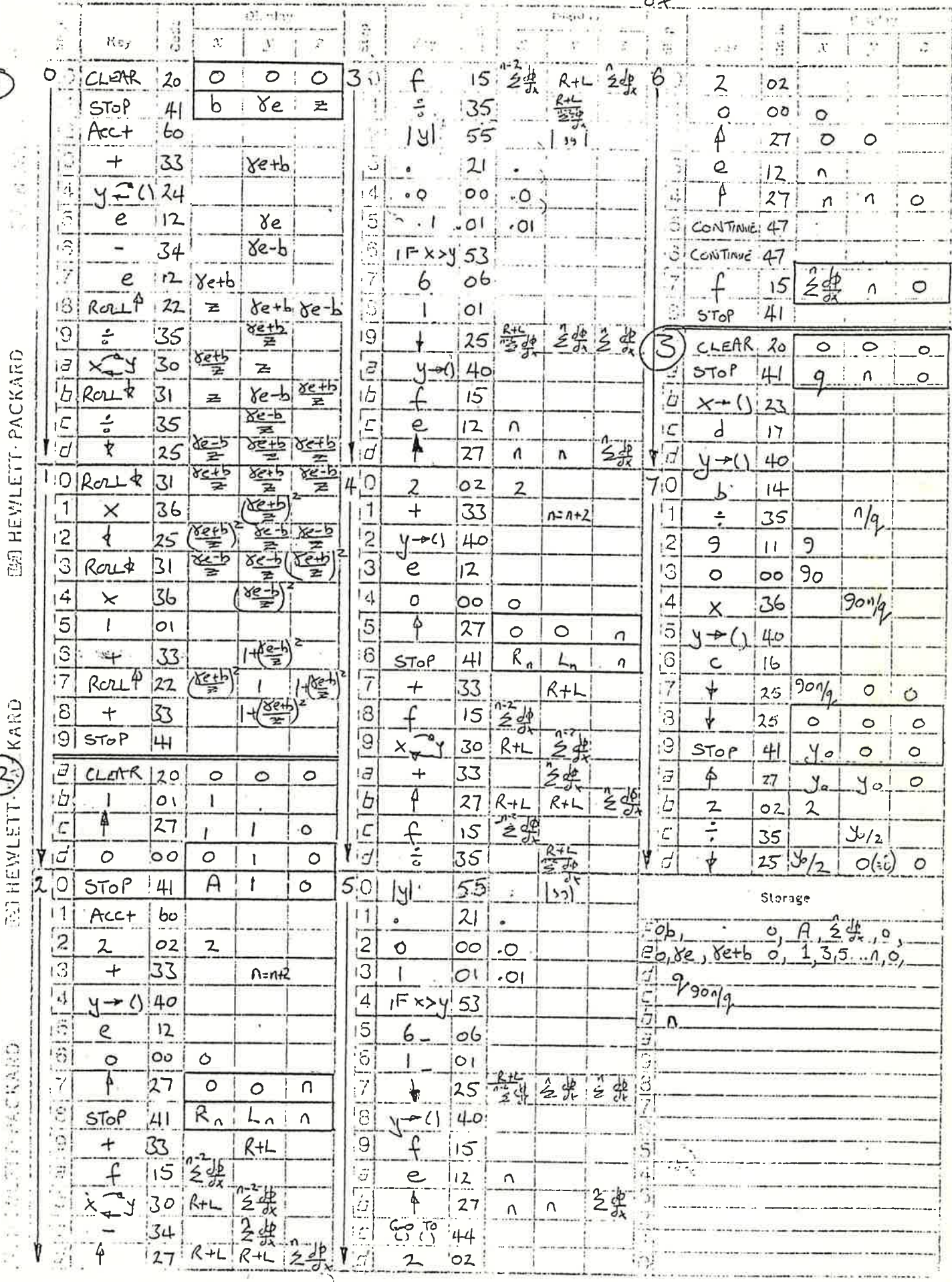

FIGURE A-4 Program Steps for Side One

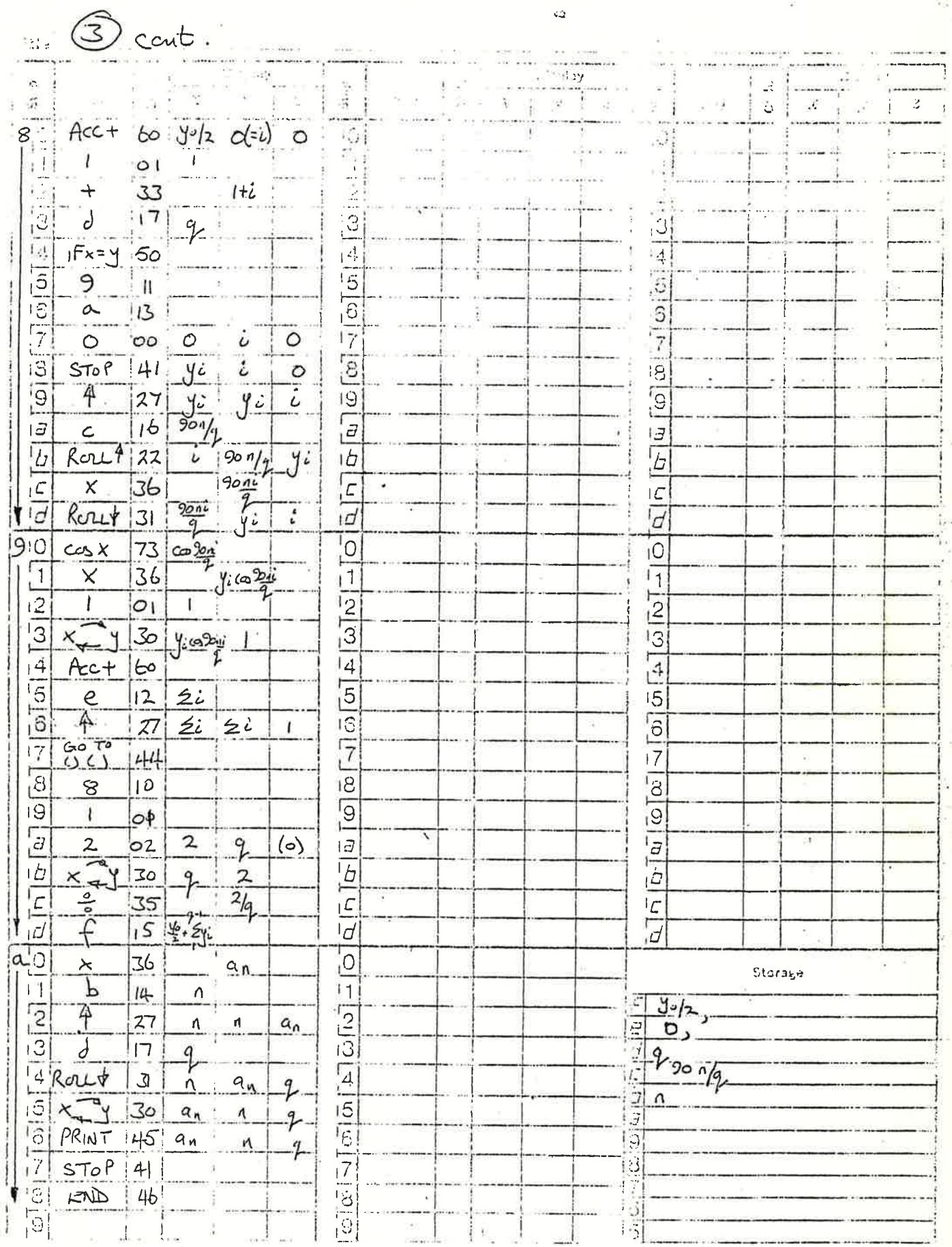

FIGURE A-4 Continued

A - 16 SIDE TWO OF MAGNETIC CARD

Title: Evaluation of $\frac{dB}{dx} \cdot \frac{10}{I}\Big|_x$ for rectangular coils. NB y, d+c registers filled before start.

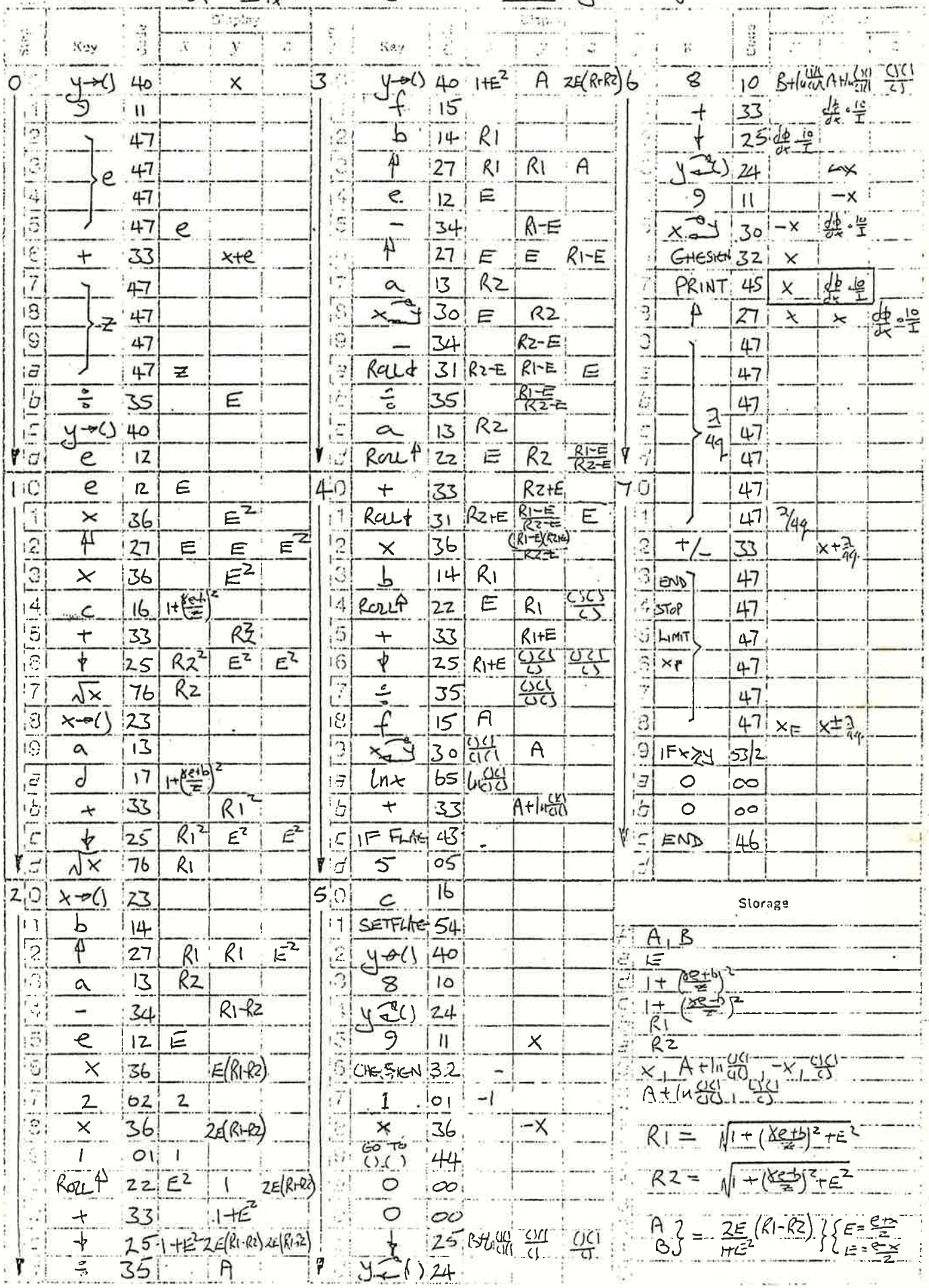

FIGURE A-5 Program Steps for Side Two

SIDE TWO, dΦ/dx for rectangular coords, cont.

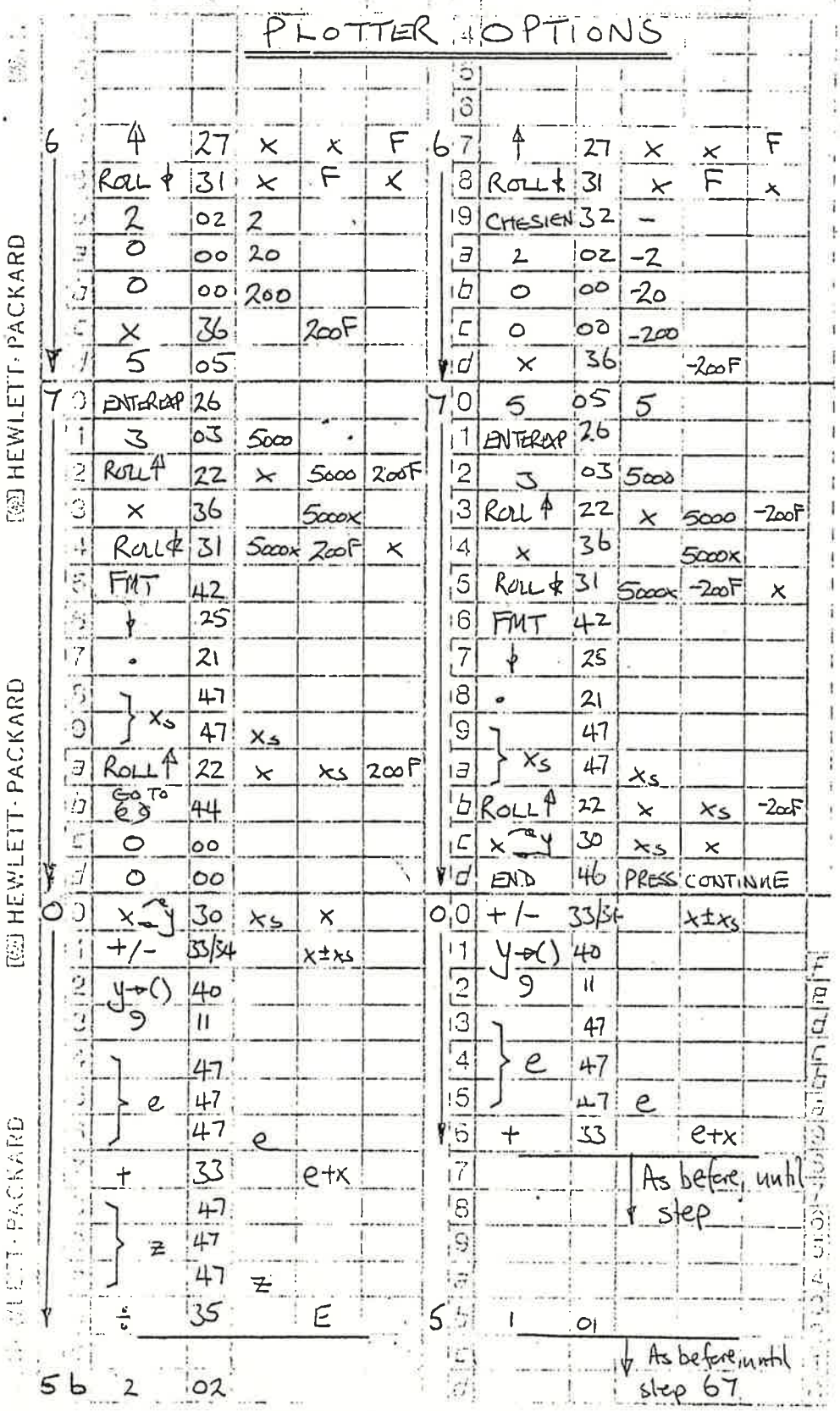

FIGURE A-5 Continued

APPENDIX V

COMPARISONS OF ALTERNATIVE MAGLEV REVENUE VEHICLE SYSTEMS

(References 134 and 135)

1. Reference 134, E. Abel, R.G. Rhodes, "Power Consumption for Alternative Maglev Systems", Electronics and Power, Vol.24, No.9, September 1978, pp.673-4.

Power consumption for alternative maglev systems

by E. Abel, B.Sc., C.Eng., M.I.E.E., and Prof. R. G. Rhodes

Two alternative systems for a high speed train are being developed in W. Germany, namely, the electrodynamic system of levitation utilising superconducting magnets and the long-stator synchronous motor for propulsion (e.d.s.), and the electromagnetic attraction system of suspension using controlled electromagnets combined with either the short-stator linear induction motor or the long-stator synchronous motor for propulsion (e.m.s.).

Edward Abel and Prof. Rhodes are with the Department of Engineering, University of Warwick, Coventry, War. CU4 7AL, England

0013-5127/78/0576 – 0673 $1.50/0

In a recent publication[1] the design details, performance characteristics and power requirements of these systems have been contrasted and compared, and the general conclusion was that the development of either system had not proceeded sufficiently far for a clear decision to be taken between them. However, it was felt that the figures quoted in the above references for the power consumption of the respective systems are somewhat misleading, in that only the active power supplied to the vehicle is considered. The complex power requirements at the wayside substations, on the other hand, have been ignored. However, when these are taken into account, particularly for the case of the linear induction machine(l.i.m.), it has a marked effect when the total powers are compared.

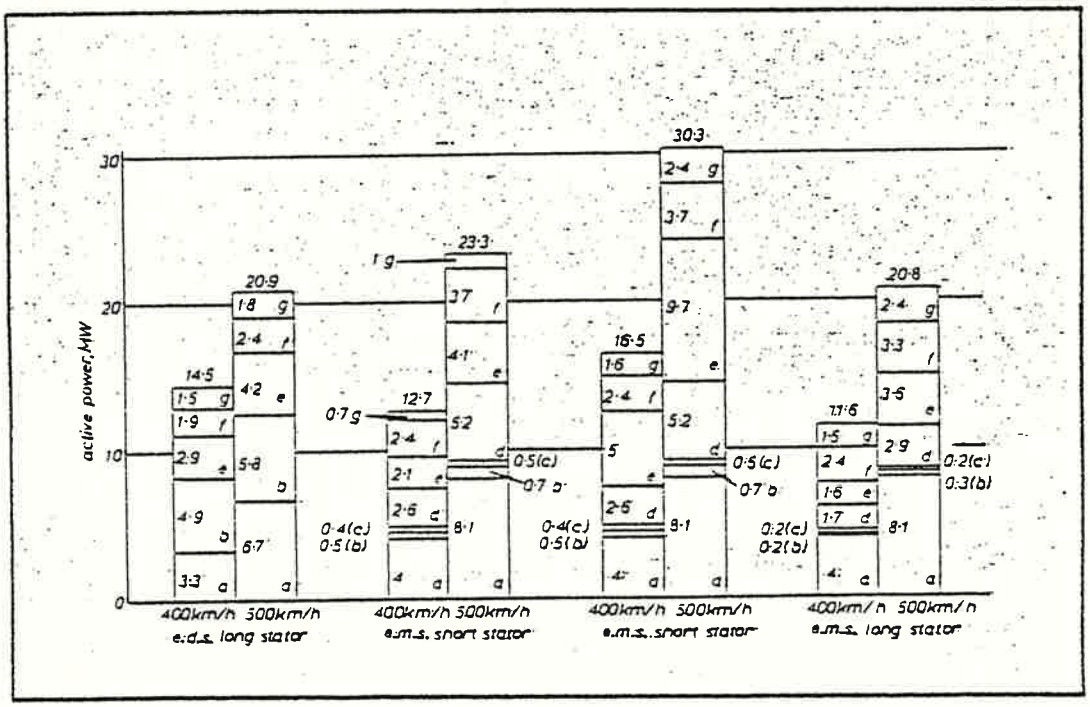

1 Total active power of systems. D.C. distribution and pickup loss not included for both e.m.s. short stator (η = 0·78 and η = 0·6, respectively)
a Aerodrag
b Magdrag (lift & guidance)
c On-board systems drag
d Remaining subsystem drag
e Subsystem losses
f Residual acceleration
g Losses from residual acceleration

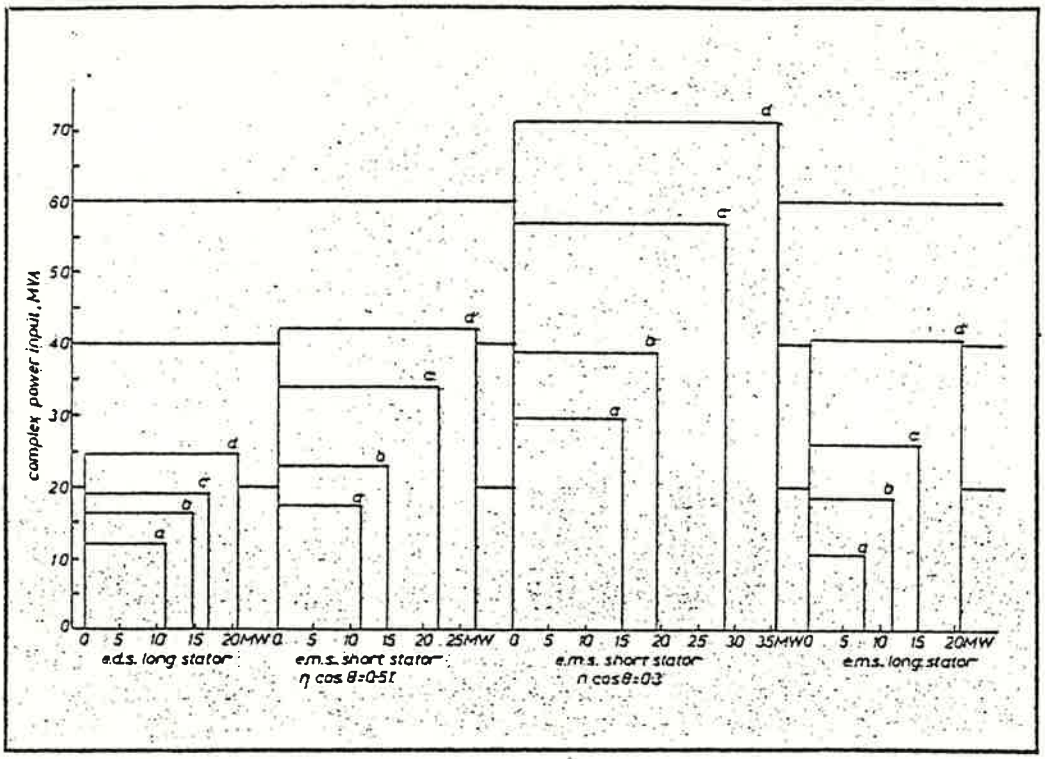

2 Total Complex and active power of systems
a 400 km/h, steady state
b 400 km/h, accelerating
c 500 km/h, steady state
d 500 km/h, accelerating

The purpose of this study was to obtain a more realistic assessment of the respective overall power requirements from published figures[1-4] for the competitive systems, and the aggregated powers are presented in the form of the block diagrams shown in Figs. 1 and 2. In assembling this data, it was discovered that very little factual information on power factor and efficiency could be found for the e.m.s. propulsion systems. However, for the purpose of calculating the complex power requirements for the short-stator l.i.m., two designs were considered with efficiencies of 0·78 and 0·60, respectively, and efficiency/power factor products of 0·51 and 0·30.

In the determination of the overall power consumption of the respective systems, the following energy requirements were considered:

- aerodynamic drag
- magnetic drag resulting from both lift and guidance
- on-board systems drag, i.e. the power supplied to the vehicle for on-board systems
- remaining steady-state drag, i.e. cooling air inlet drag
- steady-state losses (due to motor inefficiency)
- residual acceleration, i.e. extra power to accelerate against headwinds, gradients etc.
- losses from residual acceleration.

In Fig. 1 the total composite active-power requirements of the different systems have been plotted for the two speeds 400 and 500 km/h, respectively, and, in Fig. 2, both the total complex and active power requirements are presented.

It is clear from these results that the e.d.s. system with the long-stator motor (l.s.m.) propulsion requires considerably less energy than the other variants of the e.m.s. system under these assessed operating conditions. It seems equally obvious that the short-stator l.i.m. would be quite unsuitable for operational speeds of 500 km/h and even very doubtful for 400 km/h. Although the e.m.s. long-stator system would appear to have reasonable characteristics at 400 km/h, it becomes seriously degraded at 500 km/h. But it is felt that, because of the relatively meagre published information on this system, not very much reliance can be placed on these results. It can be concluded, therefore, that from the available published evidence on the relative power requirements of these proposed systems, the e.d.s. (cryogenic) design with l.s.m. propulsion (long stator) would appear to have the most promise for the required operating speeds of 400 to 500 km/h.

References

1 LEONHARD, W: 'Technische Alternativen bei der Magnetschwebebahn', *VDI Nach.*, 15th April 1977, pp. 42-43. Translated by RHODES, R.G., and RAKELS, J.H.: 'Technical alternatives for a maglev system', *Electron. & Pwr.*, 1978, 24, pp. 293-296
2 'Spurgefuhrter Fernverkehr Magnetbahnentwicklung', Proc. 6th Status Seminar des Bunderministeriums fur Forschung und Technologie, Konstanz, 1977
3 ALBRECHT, C: 'Development of levitated vehicles with superconducting magnets', *IEE Conf. Publ.* 142, 1976 pp. 113-116
4 HEBST W: 'Weight and performance characteristics of magnetically suspended high speed trains as compared to aircraft'. Presented at the 34th Conference of Society of Allied Weight Engineers, Seattle, 5th - 8th May 1975
5 WINKLE G: 'Forschungs – und Entwicklungsstand der Elektromagnetischen Schwebetechnik in der Bundesrepublik Deutschland', *ETZ-A* 1975, 96, pp. 367 - 373

2. Reference 135, E. Abel, J.L. Mahtani, R.G. Rhodes, "Linear Machine Power Requirements and System Comparisons", IEEE Transactions on Magnetics, Vol.MAG-14, No.5, September 1978, pp.918-20.

LINEAR MACHINE POWER REQUIREMENTS AND SYSTEM COMPARISONS

E. Abel*, J.L. Mahtani*, R.G. Rhodes*

ABSTRACT

The revenue vehicle designs of the two German Maglev groups are analysed and the complex power requirements at the trackside substation calculated. The two systems are the Electromagnetic System (EMS) with either linear induction motor (LIM) or long stator motor propulsion, and the Electrodynamic System (EDS) with linear synchronous motor (LSM) propulsion. The operational conditions considered were 400 and 500 km/h velocities either at steady state cruise or with a grade or headwind additional loading. It is found that the LSM of the EDS system is the most suitable form of propulsion for these operating conditions, the long stator motor for the EMS having apparently reasonable characteristics at 400 km/h, but becoming degraded at 500 km/h, and the LIM's studied being unsuited to the high speed range. These results highlight the necessity to compare not only the active power supplied to a vehicle, but also the complex power at wayside substations to be able to indicate the overall efficiencies and power factors of the competing systems.

The German, the Canadian and the Philco-Ford EDS designs are also compared by weight make-up and specific energy intensity. These results show that the advantage gained from a lightweight aircraft-type construction, coupled with the relatively longer body, is lost in the German design because of the extra dead weight of the wheel sets required for running on conventional duo-rail with the resultant heavier body structure. The respective machine power factors are included in the intensity calculations to link in reactive power storage.

INTRODUCTION

Several countries are engaged in research and development projects which employ magnetic levitation (Maglev) and linear motor or air-fan propulsion as component parts of high speed (up to 500 km/h) guided ground transport vehicles. The various systems can be divided into two major categories, the electrodynamic system (EDS) and the electromagnetic system (EMS). The main difference is that the former employ "repulsive" levitation and cryogenic magnets, and the latter "attractive" levitation and conventional iron-cored magnets. The state-of-the-art for both types of Maglev is such that system comparisons are being made between full-sized revenue-earning vehicle designs on specific routes. Because of the complexity and profusion of parameters involved it is customary to choose a few specific parameters for detailed comparison which will hopefully embody the major characteristics and performance of a system. Two parameters frequently chosen are the power-to-weight ratio of the levitation and guidance system (kW/tonne) and the specific energy intensity, (kWh/passenger-km). However, to make meaningful comparisons, the way in which other factors may dominate the choice of these and other primary parameters must be clarified.

THE GERMAN SYSTEM

The analysis and design details of the German Maglev revenue vehicles are given in the 1977 Status-seminar[1] and the basic characteristics are repeated in Table I. The vehicles are made up from two sections, the EDS design speed being 500 km/h and the EMS 400 km/h. Two propulsion schemes are considered for the EMS vehicle, i.e. the double-sided linear induction motor (LIM), and the long stator motor which also incorporates a lift function in the suspension system.

TABLE I. Characteristics of German Vehicles.

System	EDS	EMS	
Stator configuration	long	short	long
Speed, km/h	500	400	
Mass, tonnes	135	170	165
Length, m.	56	64	
No. sections	2	2	
No. passengers	200	240	
Payload, tonnes	20	24	
Height, m.	4.2	4.2	4.0
Width, m.	3.5	4.2	
Aerodynamic coefficient, m^2	3.94	4.75	
Substation spacing, km.	15	12	

A preliminary system comparison has been made of the three alternatives[2], concluding that none of the systems was sufficiently developed to allow a clear choice to be made. Although this comparison showed the power requirement at the substation, it only included the real power for the main magnetic and aerodynamic drag. Although this represents all the losses for the EDS for a given motor efficiency, no mention was made of the EMS cooling momentum drag, the short stator d.c. line loss and the long stator track iron and distribution loss, all of which appear downline from the substation. Furthermore, since the speeds of operation were also different the aerodynamic drag power would introduce a further discrepancy, e.g. an increase of speed from 400 to 500 km/h would result in a doubling of the aerodynamic dragpower. A study was performed to establish the exact power requirements of the different systems, including power factor and motor efficiency values enabling estimates of substation complex power to be made[3]. When the speed is extrapolated to 500 km/h for the EMS vehicles an additional double-sided motor is required for the short stator vehicle, and the weight is increased by 20% to 205 tonnes. The long stator design at 500 km/h requires an increase in gross weight of 10%, to 180 tonnes[1]. Operation of the EDS at the lower speed of 400 km/h should not be too far from an optimized design.

In considering the values of power factor and efficiency to use in establishing terminal conditions at the substation for the EMS vehicles, it was obvious that there were few published test results or even design figures for multi-megawatt high speed motors. Reference 4 suggests calculated efficiencies of 0.6 and 0.78 and associated power factors of 0.5 and 0.65 respectively as the first and second stage of development, and calculations have been made using both these sets of values. The breakdown of active power (Fig. 1) was:-

(1) Aerodynamic drag
(2) Magnetic drag from lift and guidance
(3) On-board system power (excluding any on-board batteries or generators).
(4) Remaining steady-state drag, viz. cooling air inlet drag.
(5) Steady-state losses due to motor inefficiency.
(6) Residual acceleration, viz. extra power to accelerate against headwinds, gradients, etc.
(7) Losses from residual acceleration.

The value of 0.013g residual acceleration was taken for the EDS in common with other values used in (1) for the EMS analysis. The systems both claim propulsion capacity for 3.5% gradients at cruise speeds. The steady-state or cruise power for the EDS is the sum of blocks 1, 2 and 3 in Fig. 1 which are the only system losses. The EMS cruise power is given by the sum of blocks 1 to 5. It must be noted that the figures used for the EMS long stator should be treated with some scepticism, if only for the reason that no largescale experimental performance characteristics have yet been reported. It is

Manuscript received March 20, 1978.

* Department of Engineering, University of Warwick, Coventry, CV4 7AL.

0018-9464/78/0900-0918$00.75 ©1978 IEEE

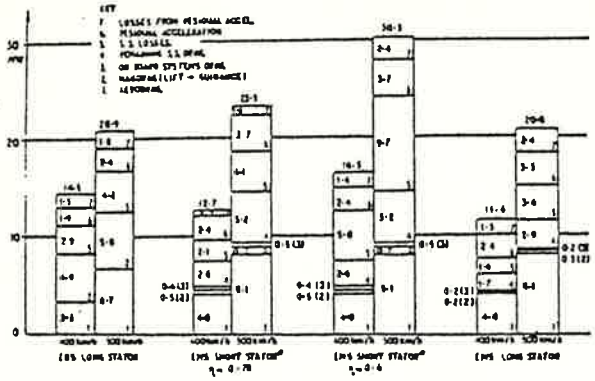

Fig. 1. Total active power of systems (MW).
Note: D.C. distribution and pickup loss not included.

apparent that, in terms of real power consumed, the long stator EMS and the EDS are both roughly equivalent when loaded at 500 km/h. The low efficiency LIM (short stator) EMS uses roughly 45% and the high efficiency LIM/EMS 11% more active power. If an estimate is also made of the D.C. line loss for the LIM, before current pickup, of 15%, the modified EMS/LIM figures are 70% and 31% respectively.

The values shown here could not have been deduced from the suspension lift-to-drag ratios or specific powers. For example the EDS 500 km/h magnetic lift-to-drag ratio of 32 (equivalent to 36 kW/tonne) is modified by aerodynamic drag so that cruise lift-to-drag becomes 15 (92 kW/tonne). Similarly, the EDS short stator magnetic specific power of 3 kW/tonne at 400 km/h (equivalent to magnetic lift-to-drag ratio of 370) is modified by the addition of aerodynamic and cooling drag to a steady-state value of 44 kW/tonne (lift-to-drag ratio of 25). The choice of a suspension subsystem with high magnetic lift-to-drag ratio does not ensure an overall high ratio because of the aerodynamic and other system losses.

TABLE II. Apparent efficiency (powerfactor - efficiency product) of the German Vehicles

	400 km/h		500 km/h	
	steady state	loaded	steady state	loaded
EDS	0.57	0.62	0.66	0.90
EMS, long stator	0.37	0.46	0.44	0.36
EMS, short stator, high efficiency	0.51	0.51	0.51	0.51
EMS, short stator, low efficiency	0.30	0.30	0.30	0.30

The change in efficiency and power factor of the three systems as loading and speed vary is indicated in Table II. The EDS system looses 7% in going from unloaded 400 km/h to loaded 500 km/h operation. A similar transition for the EMS long stator motor results in a 21% loss representing a conservative estimate as it ignores non-linearities in the iron-cored system. The short stator values were held constant as the design called for a doubling up of the motors to give sufficient thrust at the higher speed; each motor remained at much the same output, but would be operating at different slip.

The power factor of a system enables the complex power to be evaluated from a substation active power. Reactive power flow in a machine-power network is stored in the leakage inductances of the system and air gap of the machine, and as such does no useful work. However reactive power represents a power demand that has to be catered for both in plant rating and energy cost. An iron-cored structure such as a LIM or the EMS long stator motor must have a much lower power factor than a linear synchronous motor (LSM) of the same mechanical power output, since airgap magnetization is provided by superconductors requiring no input reactive power, and the armature leakage inductance is small since the track winding is air-cored. These points are born out by Figure 2, which shows the complex substation power as an ordinate against the active power for each of the four operating conditions of the systems. The success of the electrodynamic system in requiring small amounts of reactive power to provide propulsion throughout the speed and loading variation considered is apparent. The size of the ordinate, i.e. the complex power, therefore demonstrates the relative merits of the overall systems, at the substation. Despite the rough equivalence of active power used, the EMS long stator requires 38% more than the EDS base, and the high efficiency short stator 51% more. Including a line loss the LIM value rises to a 78% increase. If the lower efficiency short stator EMS is considered, then the figures become increases of 156% and 202% on the EDS 100% base.

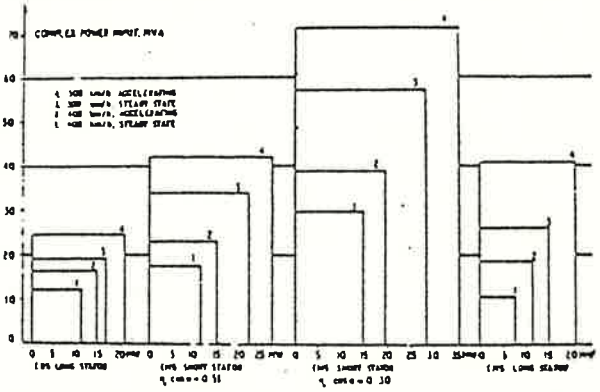

Fig. 2. Total complex and active power of systems.

From this data a power requirement comparison can be made between the three German Maglev vehicles operating under similar conditions. The comparisons cannot be strictly rigorous, since the EMS and EDS vehicles are primarily designed for different baseline operation. However, the spread of system total complex power, at the trackside substations, (Figure 2) is indicative of the type of system performance to be expected for identical service conditions. Several factors have emerged from the analysis:-

(i) The EDS has good system performance at both 500 and 400 km/h in terms of energy conversion and power consumption, and has scope for increases in power factor and efficiency, depending on economic costs of power and capital equipment.

(ii) The short stator induction machines for the EMS are quite unsuitable for high speed (500 km/h) operation, and are probably also unsuited to 400 km/h operation, primarily because of their high reactive power consumption and hence excessive overall power requirement. For example at 500 km/h the high and low-efficiency LIM's respectively required 1.8 and 3 times as much complex power as an EDS/LSM, and at 400 km/h, 1.4 and 2.4 times as much.

(iii) The long stator motor EMS appears to need marginally less power than the EDS at 400 km/h (90%), but when loaded, or at the higher speed of 500 km/h, this slight advantage is lost. Another consideration is that this machine concept has only been tested at low speed, so high-speed operating characteristics must only be regarded as tentative.

(iv) Using specific power, lift-to-drag ratio or specific energy intensity to assess system performance only indicates the active power supplied to make up thrust and losses (if included) in the system. Low power factors in the LIM systems means trackside and transmission components as well as utility energy supply costing must be in terms of total complex power used by a system. The MVA as well as the MW requirements of a system must be obtained in relation to a common guideway

route together with similar baseline specifications before reasonable comparisons can be made.

MAGLEV VEHICLE WEIGHT BREAKDOWN

Another area for comparison of vehicle data is that of weight breakdown and for this study two additional single section EDS systems are included with the German vehicle data presented in Figure 3, i.e. the Philco-Ford[5] and the Canadian[6,7] conceptual vehicle designs (see Table III). Two options are included for Philco-Ford, the baseline 80-passenger vehicle, and the 140-passenger vehicle.

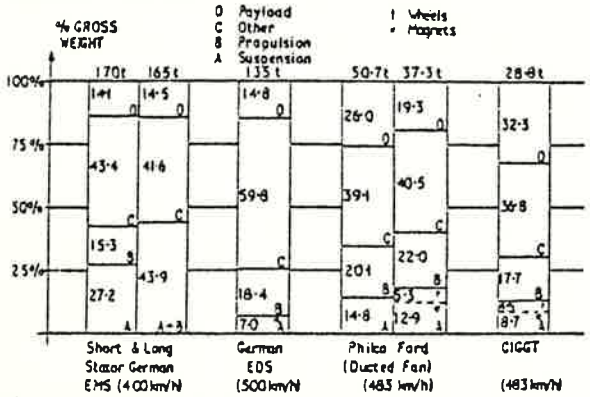

Fig. 3. Subsystem weight breakdown (% Gross).

TABLE III. Characteristics of conceptual EDS Vehicles.

System	Philco-Ford		CIGGT
Propulsion	Ducted Fan		LSM
Speed, km/h	483		483(6) 480(7)
Mass, tonnes	37.3	50.7	28.8
Length, m.	33.67	42.9	36.5
No. passengers	80	140	100
Payload, tonnes	7.2	13.2	9.3
Height, m	3.454		3.20
Width, m	2.94	3.454	3.20
Aerodynamic coefficient, m^2	1.80	2.20	2.42(6) 2.58(7)

Figure 4 shows the weight information scaled in tonnes for the six vehicles. The overall weight per seat of the German EDS vehicle compared to CIGGT and the 140 seat Philco-Ford designs is approximately double. This is largely because of the weight penalty of the heavy duo-rail compatible wheelsets opposed to lightweight aircraft-type wheels of the other EDS designs. The EMS figures for weight-per-seat demonstrate the large amount of power-conditioning and mechanical hardward in the subsystems, which is also borne out by the payload variations from 14.1% (EMS) to 32.3% (CIGGT).

SPECIFIC ENERGY INTENSITY

The specific energy intensity(Ψ) of a transport system evaluates the amount of prime energy required per passenger, per kilometer of travel. Within the calculation, the substation convertor efficiency, generation and transmission efficiency, and load factor for the vehicles are included[7]. In obtaining values for (Ψ) for non-electrical systems the heating value of the fuel and the journey stage length need to be known[5]. The values of specific energy intensity (including power factor) for the six vehicle designs considered is shown in Table IV.

The Philco-Ford values are low because of the low aerodynamic coefficients chosen together with the high magnetic lift-todrag ratio obtained with a 2.54cm thick aluminium reaction rail. In comparing the CIGGT value with the German EDS, the large vehicle weight of the

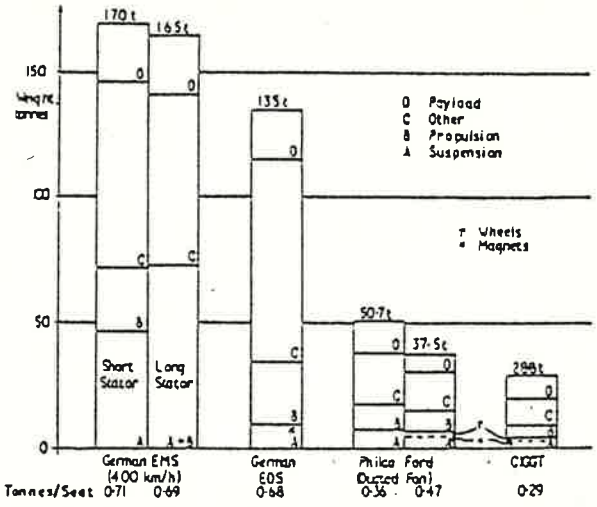

Fig. 4. Subsystem weight breakdown.

TABLE IV. Specific Energy Intensity.

System	EMS Short stator	EMS Long stator	EDS	Philco-Ford 140 pass.	Philco-Ford 80 pass	CIGGT
speed	500	500	500	483	483	480
	high η	low η				
ψ	6.51	11.2	5.1	4.45	2.75	3.63	3.72

latter has completely offset the advantage obtained by increasing the vehicle length as shown by the Philco-Ford difference between short and long vehicles. This decrease in ψ occurs since passenger number increases more rapidly than drag on the extended vehicle.

CONCLUSIONS

The study evaluates and compares total substation power required by the German revenue vehicle designs. The evidence suggests that the linear induction motor does not appear to be a good choice for a propulsion subsystem at 500 km/h or indeed at 400 km/h. The long stator motor(EMS) is likewise degraded when loaded at 400 km/h or run at 500 km/h. The EDS/LSM on the other hand appears to have the most promise for the required operating speed range of 400-500 km/h.

When compared with other EDS designs the German system is shown to be limited by its excessive dead weight as a consequence of the requirement for conventional duo-rail compatibility.

In evaluating any system it has been shown that it is necessary to completely identify the energy make-up rather than specify particular parameters such as lift-to drag ratio or specific power intensity in isolation.

REFERENCES

1. "Spurgefuhrter Fernverkehr Magnetbahnentwicklung", Proc. 6th Statusseminar des Bundesministeriums fur Forschung und Technologie, Konstanz, 1977".
2. W. Leonhard, "Technische Alternativen bei der Magnetschwebebahn", VDI Nach, No.15, 15 April 1977, pp. 42-3.
3. E. Abel, "A Study of the Power Consumption of German Maglev Passenger Vehicles, (EDS and EMS)". Internal Memo, University of Warwick, January 1978.
4. G. Winkle, "Forschungs-und Entwicklungsstand der Elektromagnetischen Schwebetechnik in der Bundesrepublik Deutschland", ETZ-A, Vol. 96, No. 9, 1975, pp. 367-73.
5. T.B. Clark, R.L. Pons. "Conceptual Design and Analysis of the Tracked Magnetically Levitated Vehicle Technology Program - Repulsion Scheme". Vol. I & II, PB 247931/2, Report Nos. FRA-OR & D-75-21-21A, US Dept. of Transportation, February 1975.
6. W.F. Hayes, "High-Speed Electrodynamic Maglev Guided Ground Transportation System Conceptual Design Study", NRC Canada, Report No. LTR-CS-176, September 1977.
7. Canadian Maglev Group, "The Canadian High Speed Magnetically Levitated Vehicle System", Summary Report, CIGGT Report No. 77-12, September 1977.